European Journal of Mechanics / B Fluids 107 (2024) 80–94

Contents lists available at ScienceDirect

European Journal of Mechanics / B Fluids

journal homepage: www.elsevier.com/locate/ejmflu

Sensitivity analysis of the Cercignani - Lampis accommodation coefficients in prototype rarefied gas flow and heat transfer problems via the Monte Carlo method

Thanasis Basdanis [*], Giorgos Tatsios [1], Dimitris Valougeorgis

Department of Mechanical Engineering, University of Thessaly, Pedion Areos, Volos 38334, Greece

ARTICLE INFO

Keywords:
Rarefied gas dynamics
Cercignani-Lampis kernel
Monte Carlo method
Uncertainty propagation
Poiseuille
Thermal creep and thermomolecular pressure difference flows
Couette and fourier flows

ABSTRACT

In rarefied gas dynamics, the Cercignani-Lampis (CL) scattering kernel, containing two accommodation coefficients (ACs), namely the tangential momentum and normal energy ones, is widely employed to characterize gas-surface interaction, particularly in non-isothermal setups, where both momentum and energy may simultaneously be exchanged. Here, a formal and detailed sensitivity analysis of the effect of the CL ACs on the main output quantities of several prototype problems, namely the cylindrical Poiseuille, thermal creep and thermomolecular pressure difference (TPD) flows, as well as the plane Couette flow and heat transfer (Fourier flow), is performed. In each problem, some uncertainties are randomly introduced in the ACs (input parameters) and via a Monte Carlo propagation analysis, the deduced uncertainty of the corresponding main output quantity is computed. The output uncertainties are compared to each other to determine the flow configuration and the gas rarefaction range, where a high sensitivity of the output quantities with respect to the CL ACs is observed. The flow setups and rarefaction regimes with high sensitivities are the most suitable ones for the estimations of the ACs, since larger modeling and experimental errors may be acceptable. In the Poiseuille and Couette flows, the uncertainties of the flow rate and shear stress respectively are several times larger than the input uncertainty in the tangential momentum AC and much smaller than the uncertainty in the normal energy AC in a wide range of gas rarefaction. In the thermal creep flow, the uncertainty of the flow rate depends on the input ones of both ACs, but, in general, it remains smaller than the input uncertainties. A similar behavior with the thermal creep flow is obtained in the TPD flow. On the contrary, in the Fourier flow, the uncertainty of the heat flux may be about the same or even larger than the input ones of both ACs in a wide range of gas rarefaction. It is deduced that in order to characterize the gas-surface interaction via the CL ACs by matching computations with measurements, it is more suitable to combine the Poiseuille (or Couette) and Fourier configurations, rather than, as it is commonly done, the Poiseuille and thermal creep ones. For example, in order to estimate the normal energy AC within an accuracy of 10 %, experimental uncertainties should be less than 4 % in the thermal creep or TPD flows, while may be about 10 % in the Fourier flow.

1. Introduction

Rarefied gas dynamics are employed in various engineering and technological fields, including gaseous microfluidics [1,2], vacuum gas technology and pumping [3,4], metrology [5], lubrication [6], porous media [7,8] and high-altitude gas dynamics [9,10]. The main unknown is the velocity distribution function, which obeys the Boltzmann equation or some suitable kinetic model equation, while the macroscopic quantities of practical interest are obtained by the moments of the distribution function. In addition, at the boundaries of the flow configuration, some kinetic-type boundary conditions must be specified. More specifically, the distribution function of the reflected gas particles is expressed with regard to that of the incident ones, which is part of the solution. Obviously, the reliable prediction of the gas-surface interaction is essential in the accurate solution of the flow setup.

At the boundaries, the relation between the incident and reflected distribution functions, denoted by $f(\boldsymbol{\upsilon}')$ and $f(\boldsymbol{\upsilon})$ respectively, with $\boldsymbol{\upsilon}'$ and $\boldsymbol{\upsilon}$ denoting the corresponding molecular velocity vectors, is expressed by

* Corresponding author.
E-mail addresses: abasdanis@mie.uth.gr (T. Basdanis), gtatsios@ed.ac.uk (G. Tatsios), diva@mie.uth.gr (D. Valougeorgis).
[1] School of Engineering, Institute of Multiscale Thermofluids, The University of Edinburgh, Edinburgh EH9 3FB, UK

https://doi.org/10.1016/j.euromechflu.2024.05.003
Received 22 March 2024; Received in revised form 25 May 2024; Accepted 31 May 2024

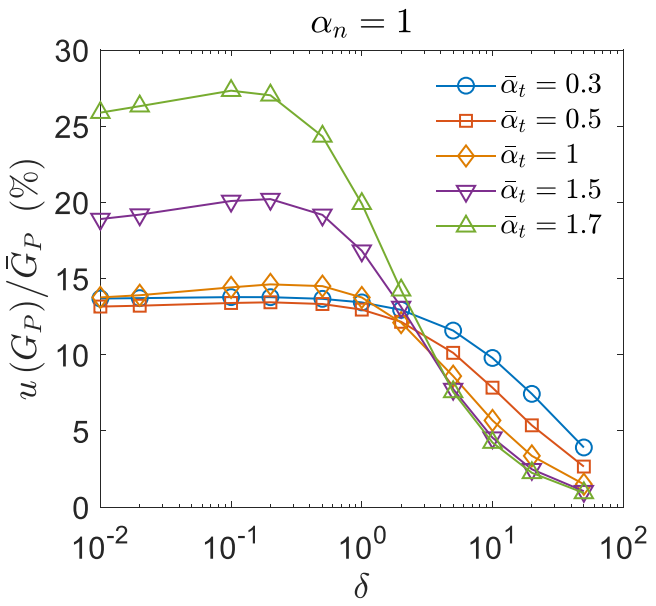

Fig. 1. Poiseuille flow – Uncertainty of reduced flow rate $u(G_P)/\overline{G}_P$ vs δ for input uncertainty $u(\alpha_t)/\overline{\alpha}_t = 10\%$, with $\bar{a}_t = [0.3, 0.5, 1, 1.5, 1.7]$ and $a_n = 1$.

means of the scattering or reflection kernel $R(\boldsymbol{\upsilon}'\!\to\!\boldsymbol{\upsilon})$ as [11]

$$|\upsilon_n| f(\boldsymbol{\upsilon}) = \int_{\upsilon'_n<0} |\upsilon'_n| f(\boldsymbol{\upsilon}') R(\boldsymbol{\upsilon}'\!\to\!\boldsymbol{\upsilon}) d\boldsymbol{\upsilon}' \tag{1}$$

In Eq. (1), υ'_n and υ_n are the components of the associated molecular velocities normal to the boundary (υ_n is always directed into the gas). The scattering kernel $R(\boldsymbol{\upsilon}'\!\to\!\boldsymbol{\upsilon})$ gives the probability that a particle which impinges the wall with velocity $[\boldsymbol{\upsilon}', \boldsymbol{\upsilon}' + d\boldsymbol{\upsilon}']$, will reflect back into the flow with velocity $[\boldsymbol{\upsilon}, \boldsymbol{\upsilon} + d\boldsymbol{\upsilon}]$. The scattering kernel must obey certain mathematical properties and usually contains one or more free parameters, the so-called accommodation coefficients (ACs), which characterize the gas-surface interaction of some property (mass, momentum, energy).

The AC of some property φ is the ratio of the actual flux of this property normal to the wall, over the corresponding one, assuming complete accommodation at the wall. Mathematically, it is defined as [12]

$$\alpha(\varphi) = \frac{\int_{\upsilon'_n<0} |\upsilon'_n| f(\boldsymbol{\upsilon}') \varphi(\boldsymbol{\upsilon}') d\boldsymbol{\upsilon}' - \int_{\upsilon_n>0} |\upsilon_n| f(\boldsymbol{\upsilon}) \varphi(\boldsymbol{\upsilon}) d\boldsymbol{\upsilon}}{\int_{\upsilon'_n<0} |\upsilon'_n| f(\boldsymbol{\upsilon}') \varphi(\boldsymbol{\upsilon}') d\boldsymbol{\upsilon}' - \int_{\upsilon_n>0} |\upsilon_n| f_{dif}(\boldsymbol{\upsilon}) \varphi(\boldsymbol{\upsilon}) d\boldsymbol{\upsilon}} \tag{2}$$

where $\varphi(\boldsymbol{\upsilon})$ is some function of $\boldsymbol{\upsilon}$ and f_{dif} is the Maxwellian distribution function, characterized by the temperature and velocity of the wall. The ACs sometimes are measured directly, but in most cases, they are extracted in an indirect manner by comparing measurements with computations based on some scattering kernel.

The gas-surface interaction is a rather complex phenomenon, affected by many factors at micro and macroscale levels. The primary factors include the surface material and its treatment, as well as the molecular mass and structure of the gas species, while other factors, such as the gas temperature and boundary shape, may also be important. All these factors, which may be present in the momentum and energy transfer between the surface and the gas, although not explicitly considered, obviously affect the evaluation of the ACs. In general, it is expected that the gas-surface interaction becomes less diffusive (more specular) as the surface is polished, the molecular mass is reduced and the temperature is increased, while the effect of pressure (or number density) is minor. These general trends are reported in many gas-surface interaction reviews [13,14], although there are several experimental and computational studies with contradicting results [15–17]. Despite the existing pitfalls and deficiencies, the implementation of scattering models with constant or molecular velocity dependent ACs remains the most common, straightforward and computationally efficient approach to provide reliable boundary conditions in kinetic modeling at mesoscale level.

Surely, the most widely employed scattering model, with considerable success, is the one proposed by Maxwell [18], mainly for either pressure driven isothermal [19–24] and non-isothermal [25] flows or purely heat transfer flows [26–28], describing the tangential momentum and energy exchange between the gas and the surface respectively. The main shortcoming of the Maxwell model is that it contains only one free parameter, which remains the same for all accommodation modes, i.e. for any $\varphi(\boldsymbol{\upsilon})$, and therefore, cannot properly characterize the gas-surface interaction in rarefied gas flows with coupled momentum and energy transfer.

The second most widely employed scattering model is the one proposed by Cercignani & Lampis, given by [29]

$$R(\boldsymbol{\upsilon}'\!\to\!\boldsymbol{\upsilon}) = \frac{m^2|\upsilon_n|}{2\pi a_n a_t (2-a_t)(kT_w)^2} I_0\left(\frac{m\sqrt{1-a_n}\upsilon_n\upsilon'_n}{a_n kT_w}\right) \times \exp\left[-\frac{m\left[\upsilon_n^2 + (1-a_n)\upsilon_n'^2\right]}{2kT_w a_n} - \frac{m[\boldsymbol{\upsilon}_t - (1-a_t)\boldsymbol{\upsilon}'_t]^2}{2kT_w a_t(2-a_t)}\right] \tag{3}$$

In Eq. (3), υ'_n and υ_n are the components of the incident and reflected molecular velocity normal to the boundary, while $\boldsymbol{\upsilon}'_t = [\upsilon'_{t1}, \upsilon'_{t2}]$ and $\boldsymbol{\upsilon}_t = [\upsilon_{t1}, \upsilon_{t2}]$ are the corresponding two-dimensional vectors tangential to the boundary. Also, m is the molecular mass, k is the Boltzmann constant, T_w is the surface temperature and $I_0(x) = (1/2\pi)\int_0^{2\pi} \exp(x\cos\psi)\, d\psi$ is the modified Bessel function of the first kind and zeroth order. The Cercignani-Lampis (CL) model contains two ACs, namely $\alpha_t \in [0, 2]$ and $\alpha_n \in [0, 1]$, which correspond to the tangential momentum and normal energy that the molecules exchange with the surface during the interaction. By substituting the CL kernel into Eq. (1) and the resulting expression into Eq. (2), with $\varphi(\boldsymbol{\upsilon}) = m\upsilon_t$ and $\varphi(\boldsymbol{\upsilon}) = m\upsilon_n^2/2$, it is deduced, in a straightforward manner, that $\alpha(m\upsilon_t) = \alpha_t$ and $\alpha(m\upsilon_n^2/2) = \alpha_n$ [30]. Thus, α_t and α_n have clear physical meaning. Also, it is worth noting that if the same manipulation is repeated, with $\varphi(\boldsymbol{\upsilon}) = m\upsilon_t^2/2$, it is readily reduced that $\alpha(m\upsilon_t^2/2) = a_t(2-a_t)$ [31], implying that when α_t is fixed, both the tangential momentum and tangential energy accommodation modes are specified. This is probably a pitfall of the CL model, since there is no physical reasoning that these two modes are somehow connected, but in any case, compared to the Maxwell model, the CL kernel is more versatile, since it is possible to distinguish between momentum and energy accommodation [32]. In addition, back-scattering investigation is feasible [33], plume-like structures of re-emitted molecules may be recovered [11] and the exponent in the thermomolecular pressure difference (TPD) effect, in the free molecular limit, can take values of less than 0.5, which is in agreement with experimental data (the free molecular value obtained by the Maxwell model is always 0.5 independent of the AC) [34,35]. Thus, the CL kernel has been extensively employed to computationally solve non-isothermal internal [30,35–41] and external [42–47] rarefied gas flows in a wide range of α_t and α_n in order to investigate the effect of the gas-surface interaction on the output quantities.

In parallel, there has been significant effort to determine the ACs of the CL model for a variety of gas-surface combinations by comparing numerical results with experimental data [33,35,36,38,39,48–50]. To obtain a unique pair of ACs in a wide range of gas rarefaction, at least two different types of flows for the same gas and surface material must be examined. Of course, the numerical results should be based on the same kinetic formulation, while measurements, ideally, should be performed in the same experimental rig. In most cases, fully-developed flows through long capillaries of circular or rectangular cross sections are considered [19,49,51–59]. First, the tangential momentum AC, α_t, is extracted by considering fully developed isothermal pressure driven flow. In these Poiseuille type flows, the exchange of tangential momentum between gas

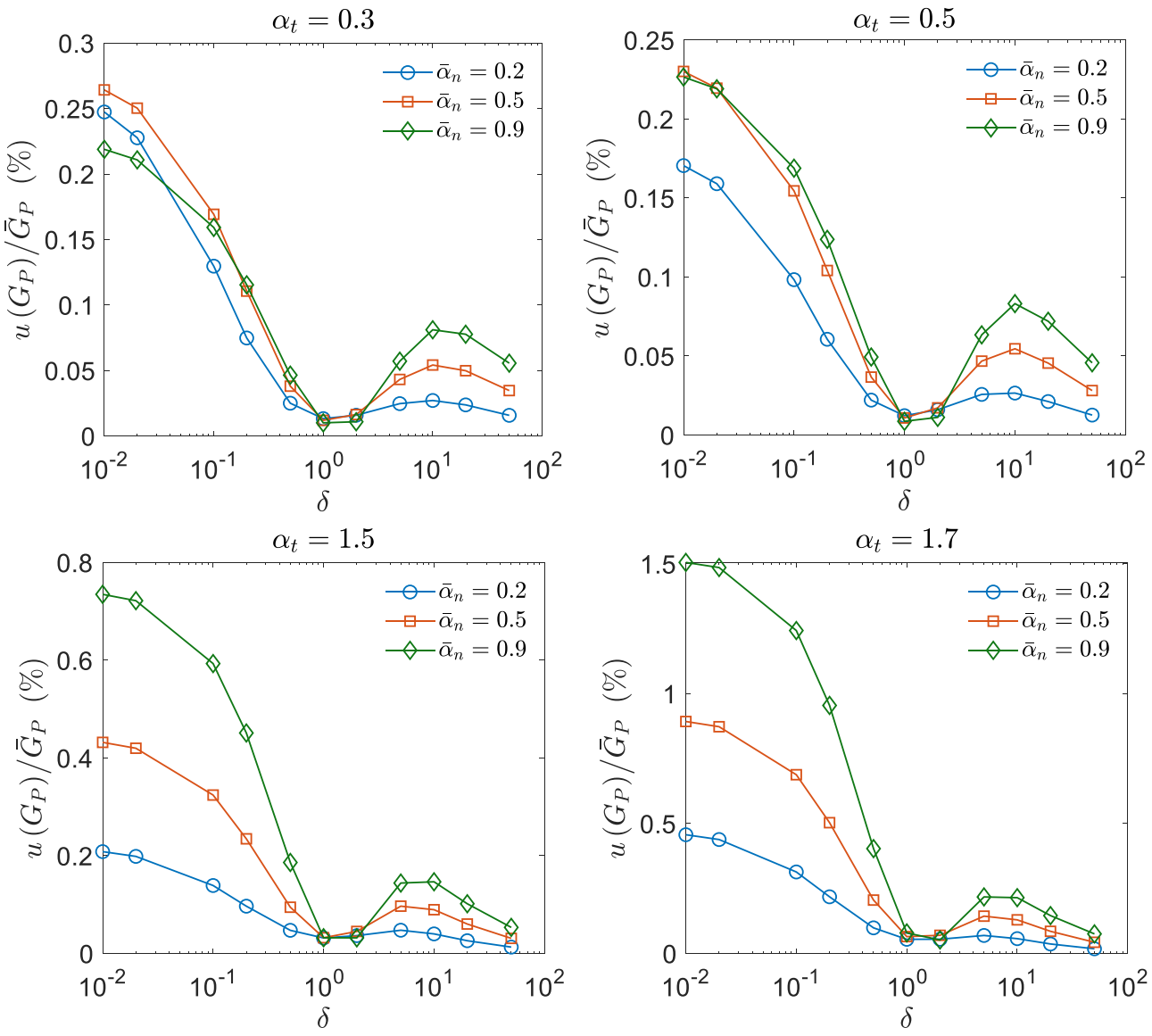

Fig. 2. Poiseuille flow – Uncertainty of reduced flow rate $u(G_P)/\bar{G}_P$ vs δ for input uncertainty $u(\alpha_n)/\bar{\alpha}_n = 10\%$, with $\bar{\alpha}_n = [0.2,\ 0.5,\ 0.9]$ and $\alpha_t = [0.3, 0.5,\ 1.5, 1.7]$.

particles and surrounding surfaces is expected to be much larger than the normal energy exchange, which is in agreement with the results obtained by the CL model, where the computed flow rate depends only on α_t and is actually independent of α_n. Thus, α_t is fixed, while α_n remains a free parameter. Then, by considering fully-developed temperature driven flow, namely thermal creep flow or alternatively TPD (either of them depends on both ACs) the normal energy AC, α_n, is extracted (α_t is kept fixed). The matching between experimental and numerical data is based in the thermal creep flow on the mass flow rate and in the TPD effect on the established downstream to upstream pressure ratio in order to have zero net mass flow rate.

The reported experimental work with rarefied, isothermal, Poiseuille type flows is extensive. The mass flow rate is deduced by measuring the pressure variation in the upstream and downstream vessels, located at the two ends of the long capillary, and employing mass conservation. In general, the estimated experimental uncertainties of the mass flow rate are small, allowing accurate estimation of α_t. For example, uncertainties of less than 4.5 % in [52–54], less than 6 % in [49] and less than 0.5 % in [59], are reported.

The corresponding mass flow rate measurements, either in thermal creep or TPD, are based on a similar methodology as in pressure driven flows, but they are cumbered due to significantly increased experimental complexity and uncertainties. Additional instrumentation is needed for the accurate measurement of the imposed temperature gradient along the flow. The significant reduction of the mass flow rate in the TPD flow as the gas rarefaction decreases and the relatively small pressure deviations in TPD, compared to pressure driven flows, require more precise instruments and measurements to reduce experimental uncertainties. Furthermore, very accurate measurement of the actual dimensions of the microchannel cross sections is needed. Certainly, it would greatly help to perform experimental work in highly rarefied regimes, but in this case, the experimental rig is more sensitive to potential leaks and outgassing, which should be accordingly treated.

Therefore, the reported experimental work is rather limited, and the associated estimated uncertainties are much larger. In particular, uncertainties of about 10 % and even larger at small values of the rarefaction parameter are reported in [56] and up to 12 % in [49], while uncertainties which may exceed 8 % are reported in the computed thermal slip coefficients in [58]. In addition to the experimental difficulties, it is important to note that the dependency of the mass flow rate in thermal creep flow or of the pressure ratio in the TPD effect on α_n is rather weak, particularly for α_t close to one or when the flow is in the slip

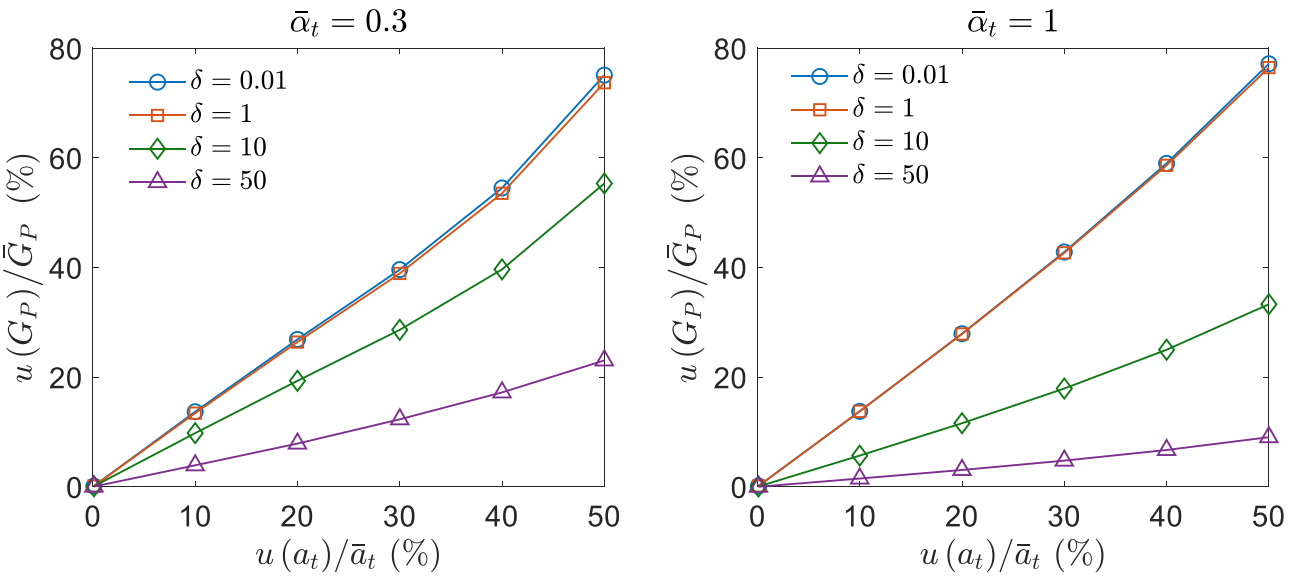

Fig. 3. Poiseuille flow – Uncertainty of reduced flow rate $u(G_P)/\overline{G}_P$ vs $u(\alpha_t)/\overline{\alpha}_t$, with $\overline{\alpha}_t = [0.3, 1]$ and $\alpha_n = 1$ for $\delta = [10^{-2},\ 1,\ 10,\ 50]$.

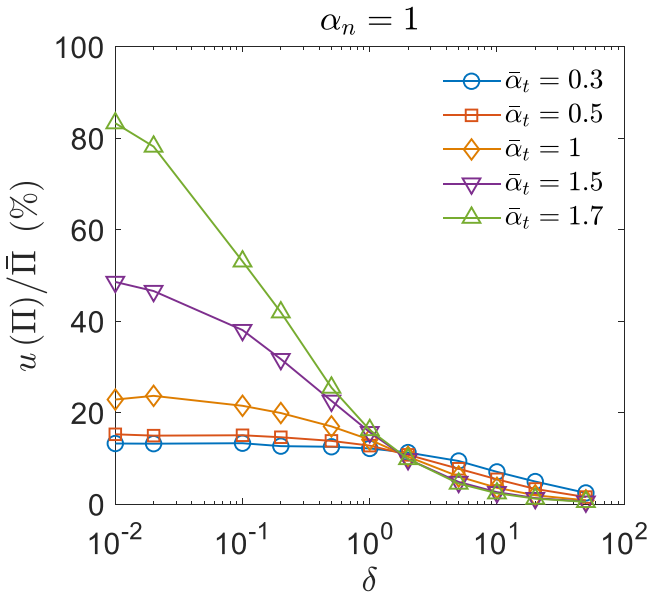

Fig. 4. Couette flow – Uncertainty of dimensionless shear stress $u(\Pi)/\overline{\Pi}$ vs δ for input uncertainty $u(\alpha_t)/\overline{\alpha}_t = 10\%$, with $\overline{\alpha}_t = [0.3, 0.5,\ 1,\ 1.5, 1.7]$ and $\alpha_n = 1$.

regime. Thus, although there have been several attempts to extract the CL ACs by considering fully-developed pressure and temperature driven flows, the results so far are not satisfactory, i.e., it is not possible to match corresponding numerical and experimental data in a wide range of gas rarefaction, with a unique pair of (α_t, α_n). For example, in [48,60] the reported values of the CL ACs refer only to the slip regime, while in [38,39], two significantly different pairs of (α_t, α_n) are deduced in order to match measurements and computations in the transition and slip regimes. It is noted that in [38,39], modeling uncertainties have been minimized as much as possible, by solving the linearized Boltzmann equation with advanced intermolecular potentials. It seems that in order to efficiently extract the CL ACs, either the experimental uncertainties of Poiseuille and thermal creep type flows must be further reduced, or other combinations of flow setups must be examined.

Alternative flow combinations may include boundary driven flows (e.g. Couette flow) or heat transfer between parallel plates or coaxial cylinders (Fourier flow). In particular, in the latter case, the reported dependency of the heat flux on both α_t and α_n is strong in a wide range of gas rarefaction including the slip regime [41]. Thus, it may be reasonable to combine isothermal pressure or boundary driven flows with Fourier type flows in order to characterize the tangential momentum and normal energy exchange between the gas and the surface via the CL model. Other scattering kernels to relate incident and reflected distribution functions are available but they are not easy to use, at least for general purposes, because they contain three or more free parameters [38,61,62].

Based on the above discussion, in the present work, the effect of the CL ACs on the overall output quantities of several representative prototype rarefied gas flow and heat transfer problems is quantified by conducting a formal sensitivity analysis. The problems include the cylindrical Poiseuille and thermal creep flows and TPD effect, as well as the plane Couette and Fourier flows. They are all simulated based on the linearized Shakhov (S) kinetic equation [63] with CL boundary conditions. It is noted that although these problems have been solved using the CL boundary conditions, so far, a uniform formal sensitivity analysis to quantitatively determine the effect of the CL ACs on the output quantities has not been performed. This is the objective of the present work and it is fulfilled by introducing some uncertainty in α_t and α_n (input parameters) and computing the deduced uncertainty in the main output quantity of each problem via the Monte Carlo method (MC) [64,65]. Obviously, for a given input uncertainty, as the output uncertainty increases, the dependency of the output quantity on α_t or α_n becomes stronger. Identifying the flow configuration and the gas rarefaction regime, where the impact of the CL ACs is expected to be more dominant is certainly beneficial in future experimental work and in the characterization of targeted gas-surface combinations, as well as in the design of systems operating under vacuum conditions.

The rest of the paper is organized as follows: In Section 2, the kinetic formulation (linearized S model with CL boundary conditions) of all problems is provided, while in Section 3, the MC uncertainty propagation analysis is described. In Section 4, the computed uncertainties in the output quantities versus the input ones in the whole range of gas rarefaction are presented and discussed. The output quantities include the flow rates in the Poiseuille and thermal creep flows, the exponent in the TPD effect, the shear stress in the Couette flow and the heat flux in the Fourier flow. Finally, in Section 5, the main concluding remarks are outlined.

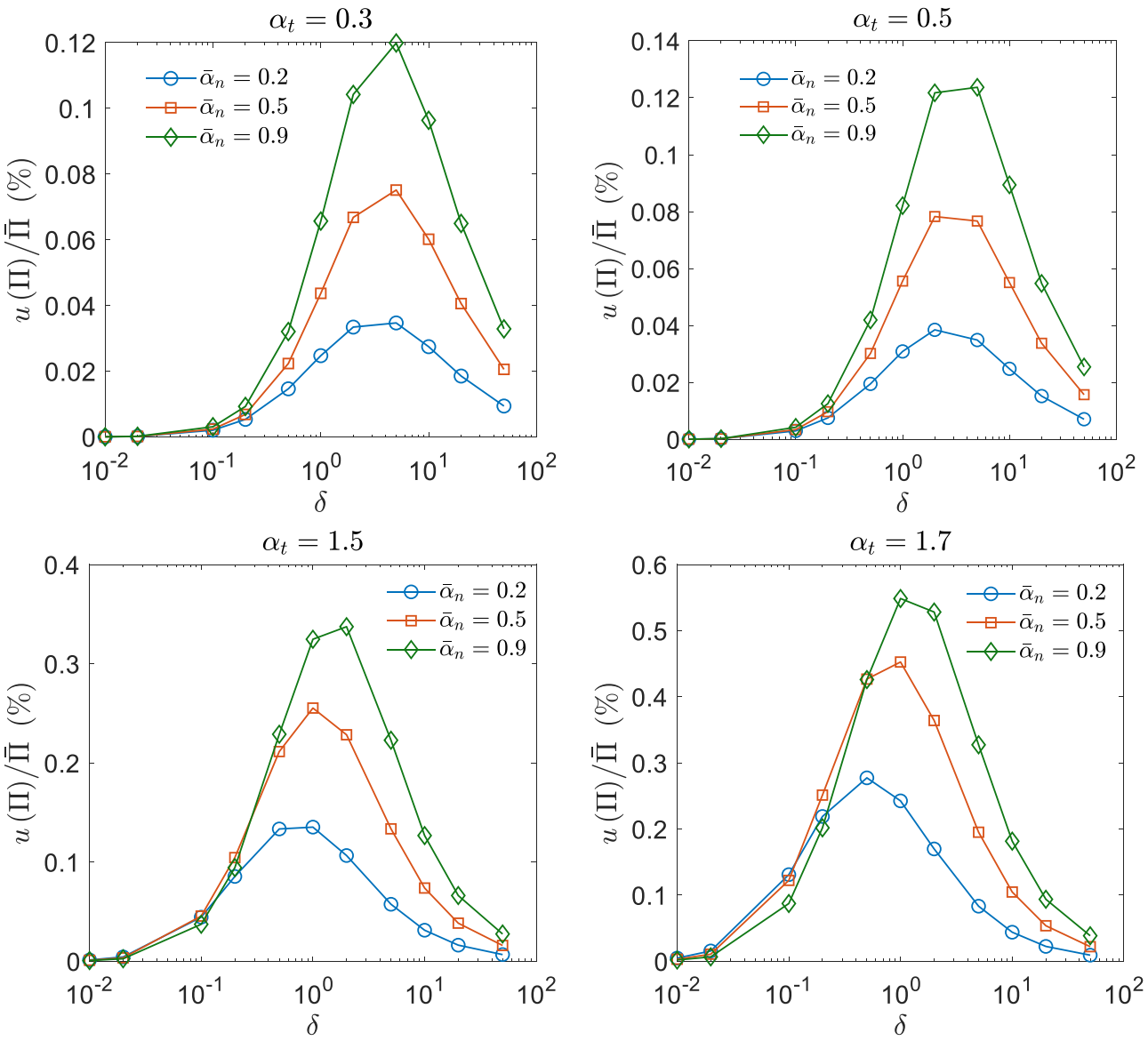

Fig. 5. Couette flow – Uncertainty of dimensionless shear stress $u(\Pi)/\overline{\Pi}$ vs δ for input uncertainty $u(\alpha_n)/\bar{\alpha}_n = 10\%$, with $\bar{\alpha}_n = [0.2,\ 0.5,\ 0.9]$ and $\alpha_t = [0.3, 0.5, 1.5, 1.7]$.

2. Kinetic formulation of the examined prototype flow setups

The investigated prototype flow configurations include linear cylindrical Poiseuille and thermal creep flows and TPD effect, as well as plane Couette and Fourier flows. The first three problems are very common in internal rarefied gas flows, while the other two have been chosen, as representative problems in boundary driven flows (Couette) and heat transfer configurations (Fourier). These flows have been extensively considered in the literature and therefore, here, only the governing linearized S kinetic equations, with the associated moments and the employed CL boundary conditions are presented, mainly for clarity and completeness. In all cases, the solutions depend on α_t and α_n, as well as on the gas rarefaction parameter $\delta = D/l$, where D is a characteristic dimension and l the equivalent mean free path, defined as $l = P/(\mu v_0)$ (P is a reference pressure, μ and v_0 are the dynamic viscosity and the gas most probable molecular speed respectively at some reference temperature) [58]. The gas rarefaction parameter $\delta \in [0, \infty)$ is proportional to the inverse Knudsen number. Formulation and most of the results are presented in dimensionless form.

Starting with the linear fully-developed cylindrical Poiseuille and thermal creep flows, following linearization and projection, the governing equations are [36]:

$$c_r\frac{\partial \Phi_i}{\partial r} - \frac{c_\theta}{r}\frac{\partial \Phi_i}{\partial \theta} + \delta\Phi_i = \delta\left[u_i + \frac{2}{15}q_i\left(c_r^2 + c_\theta^2 - 1\right)\right] + S_{\Phi_i} \tag{4}$$

$$c_r\frac{\partial Y_i}{\partial r} - \frac{c_\theta}{r}\frac{\partial Y_i}{\partial \theta} + \delta Y_i = \delta\frac{4}{15}q_i + S_{Y_i} \tag{5}$$

In Eqs. (4) and (5), $r \in [0, 1]$ is the radial coordinate, c_r and c_θ are the velocity components in the r and θ (vertical to r) directions respectively, the subscript $i = P, T$ refers to the Poiseuille and thermal creep flows and the source terms are: $S_{\Phi_P} = -1/2$, $S_{\Phi_T} = -1/2\left(c_r^2 + c_\theta^2 - 1\right)$, $S_{Y_P} = 0$, $S_{Y_T} = -1$. The bulk velocity $u_i(r)$ and heat flux $q_i(r)$ are given as

$$u_i(r) = \frac{1}{\pi}\int_{-\infty}^{\infty}\int_{-\infty}^{\infty}\Phi_i(r, c_r, c_\theta)\exp\left(-c_r^2 - c_\theta^2\right)dc_r dc_\theta \tag{6}$$

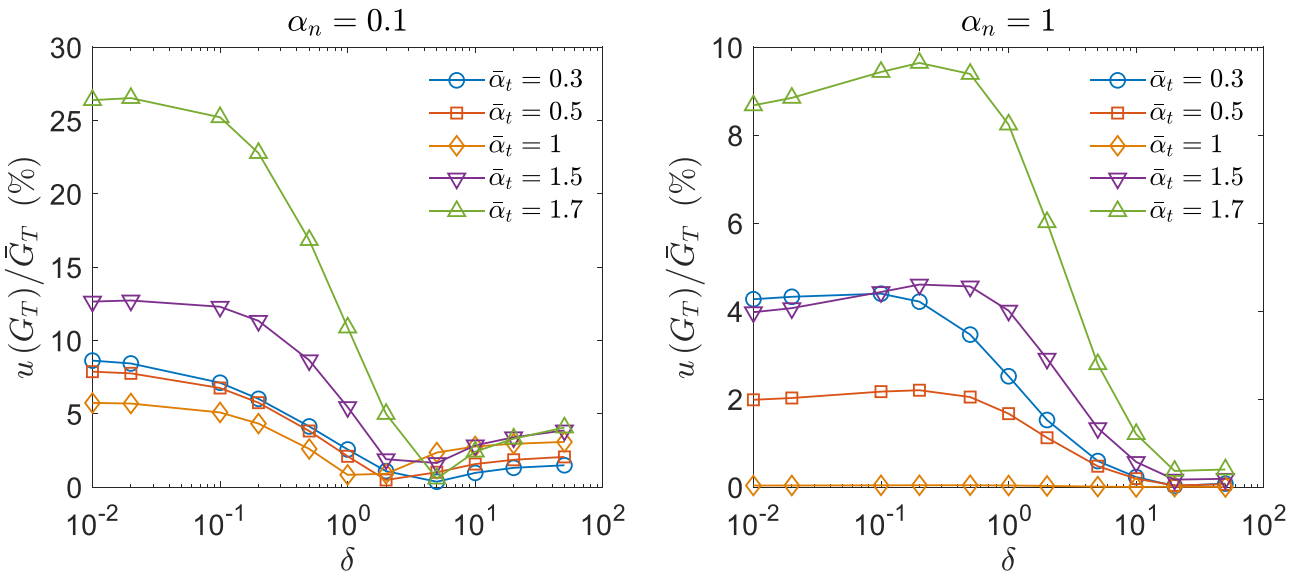

Fig. 6. Thermal creep flow – Uncertainty of reduced flow rate $u(G_T)/\overline{G}_T$ vs δ for input uncertainty $u(\alpha_t)/\overline{\alpha}_t = 10\%$, with $\overline{\alpha}_t = [0.3, 0.5,\ 1,\ 1.5, 1.7]$ and $\alpha_n = [0.1,\ 1]$.

$$q_i(r) = \frac{1}{\pi}\int_{-\infty}^{\infty}\int_{-\infty}^{\infty}\left[\Phi_i(r,c_r,c_\theta)\left(c_r^2+c_\theta^2-1\right)+\frac{3}{4}Y_i(r,c_r,c_\theta)\right] \times \exp\left(-c_r^2-c_\theta^2\right)dc_r dc_\theta \tag{7}$$

At $r = 1$, the CL boundary conditions read as:

$$\Phi_i(1,c_r<0,c_\theta) = \frac{2(1-\alpha_t)}{\alpha_n\sqrt{\pi\alpha_t(2-\alpha_t)}}\int_{-\infty}^{\infty}\int_{0}^{\infty}\Phi_i(1,c'_r>0,c'_\theta)c'_r \times \exp\left[-\frac{c'^2_r+(1-\alpha_n)c_r^2}{\alpha_n}-\frac{\left[(1-\alpha_t)c_\theta-c'_\theta\right]^2}{\alpha_t(2-\alpha_t)}\right] \times I_0\left(\frac{2\sqrt{1-\alpha_n}c_r c'_r}{\alpha_n}\right)dc'_r dc'_\theta \tag{8}$$

$$Y_i(1,c_r<0,c_\theta) = \frac{2(1-\alpha_t)^3}{\alpha_n\sqrt{\pi\alpha_t(2-\alpha_t)}}\int_{-\infty}^{\infty}\int_{0}^{\infty}Y_i(1,c'_r>0,c'_\theta)c'_r \times \exp\left[-\frac{c'^2_r+(1-\alpha_n)c_r^2}{\alpha_n}-\frac{\left[(1-\alpha_t)c_\theta-c'_\theta\right]^2}{\alpha_t(2-\alpha_t)}\right] \times I_0\left(\frac{2\sqrt{1-\alpha_n}c_r c'_r}{\alpha_n}\right)dc'_r dc'_\theta \tag{9}$$

At $r = 0$, the common symmetry boundary condition is imposed. Eqs. (4)-(9) are solved and then, the reduced flow rates (or kinetic coefficients) G_P and G_T are computed as

$$G_P = -4\int_0^1 u_P(r)rdr,\ G_T = 4\int_0^1 u_T(r)rdr \tag{10}$$

The corresponding mass flow rates may be readily deduced via a well-known methodology [12].

In the TPD effect, the net mass flow rate is zero due to a thermal creep flow in one direction and a Poiseuille flow in the opposite one. In the case of small temperature difference between the capillary ends, the exponent γ of the TPD effect may be readily deduced as

$$\gamma = \frac{G_T}{G_P} \tag{11}$$

where G_P and $G_T$are obtained by solving the Poiseuille and thermal creep flows. Depending on the experimental rig and measurement methodology, it may be easier to measure the pressure difference in a TPD setup (zero net mass flow rate), rather than the mass flow rate in a typical thermal creep flow [13]. In order to be consistent with the terminology "flow" used in the Poiseuille, Couette, thermal creep and Fourier flows, in the rest of the paper, the TPD effect will be referred as the TPD flow and the associated exponent as the TPD exponent.

In the linear Couette flow, the lower and upper plates are moving in the opposite direction with dimensionless velocities $1/2$ and $-1/2$ respectively. Following linearization and projection the governing equations are [66]:

$$c_x\frac{\partial\Phi_C}{\partial x}+\delta\Phi_C = \delta\left[u_C+\frac{2}{15}q_C\left(c_x^2-\frac{1}{2}\right)\right] \tag{12}$$

$$c_x\frac{\partial Y_C}{\partial x}+\delta Y_C = \delta\frac{4}{15}q_C \tag{13}$$

In Eqs. (12) and (13), $x \in [-1/2, 1/2]$ is the space coordinate, c_x is the x − component of the molecular velocity (normal to the walls) and $u_C(x)$, $q_C(x)$ are the bulk velocity and heat flux distributions given as

$$u_C(x) = \frac{1}{\sqrt{\pi}}\int_{-\infty}^{\infty}\Phi_C(x,c_x)\exp\left(-c_x^2\right)dc_x \tag{14}$$

$$q_C(x) = \frac{1}{\sqrt{\pi}}\int_{-\infty}^{\infty}\left[\Phi_C(x,c_x)\left(c_x^2-\frac{1}{2}\right)+Y_C(x,c_x)\right]\ \exp\left(-c_x^2\right)dc_x \tag{15}$$

At $x = \mp 1/2$, the CL boundary conditions read as:

$$\Phi_C(\mp 1/2, c_x \gtrless 0) = \pm\frac{\alpha_t}{2}+\frac{2(1-\alpha_t)}{\alpha_n}\int_{c'_x\lesseqgtr 0}|c'_x|\exp\left(-\frac{c'^2_x+(1-\alpha_n)c_x^2}{\alpha_n}\right) \times I_0\left(\frac{2\sqrt{1-\alpha_n}c_x c'_x}{\alpha_n}\right)\Phi_C(\mp 1/2, c'_x \lesseqgtr 0)dc'_x \tag{16}$$

$$Y_C(\mp 1/2, c_x \gtrless 0) = \frac{2(1-\alpha_t)^3}{\alpha_n}\int_{c'_x\lesseqgtr 0}|c'_x|\exp\left(-\frac{c'^2_x+(1-\alpha_n)c_x^2}{\alpha_n}\right) \times I_0\left(\frac{2\sqrt{1-\alpha_n}c_x c'_x}{\alpha_n}\right)Y_C(\mp 1/2, c'_x \lesseqgtr 0)dc'_x \tag{17}$$

The main output quantity is the shear stress given by

$$\Pi = \varpi(x) = \frac{2}{\sqrt{\pi}}\int_{-\infty}^{\infty}c_x\Phi_C(x,c_x)\exp\left(-c_x^2\right)dc_x \tag{18}$$

and is independent of x.

Finally, in the linear plane Fourier flow, the lower and upper plates are kept in different dimensionless temperatures $1/2$ and $-1/2$ respectively and the governing equations are [67]:

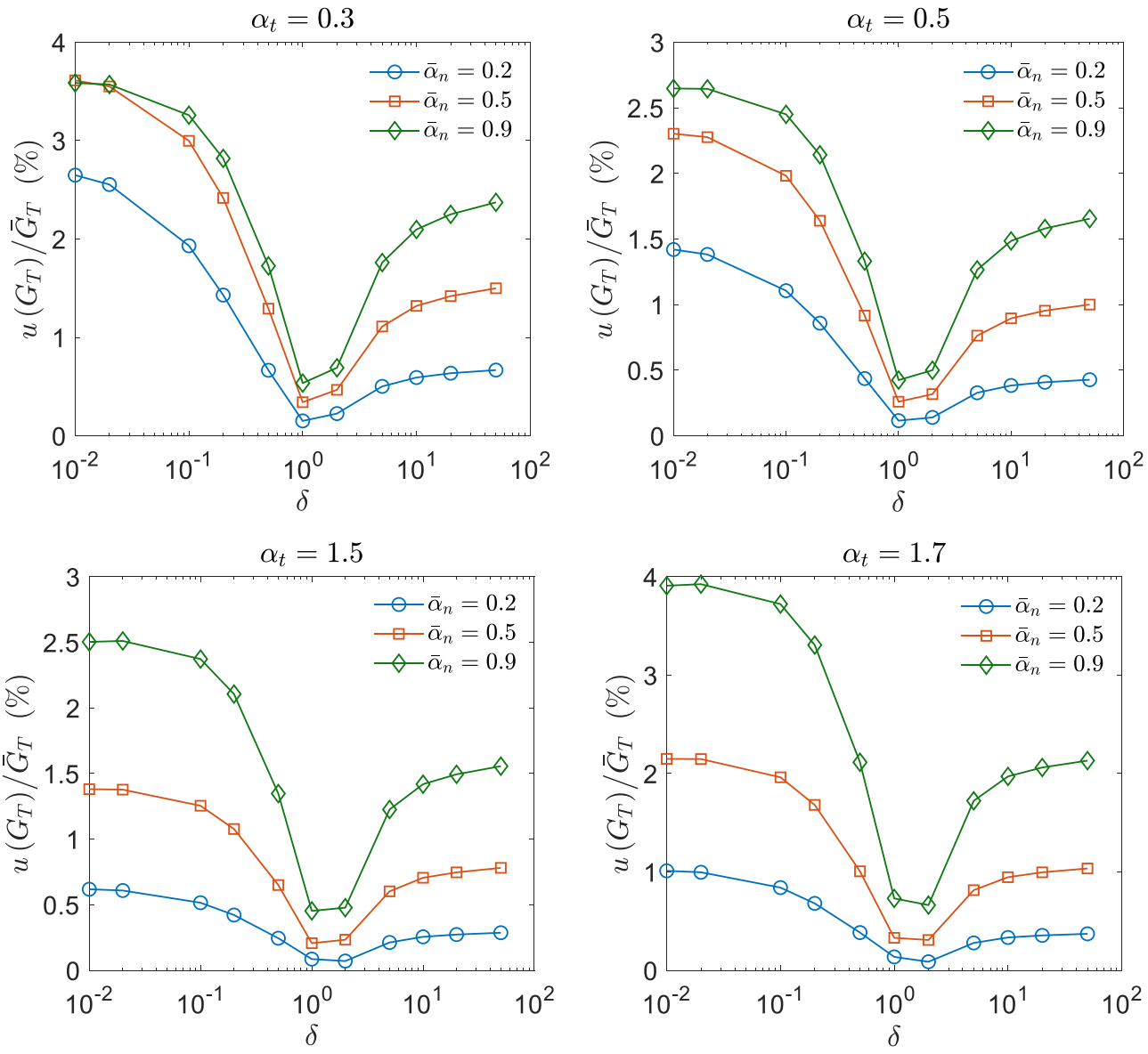

Fig. 7. Thermal creep flow – Uncertainty of reduced flow rate $u(G_T)/\overline{G}_T$ vs δ for input uncertainty $u(\alpha_n)/\overline{\alpha}_n = 10\%$, with $\overline{\alpha}_n = [0.2,\ 0.5, 0.9]$ and $\alpha_t = [0.3, 0.5,\ 1.5, 1.7]$.

$$c_x\frac{\partial \Phi_F}{\partial x} + \delta\Phi_F = \delta\left[\rho_F + \tau_F\left(c_x^2 - \frac{1}{2}\right) + \frac{4}{15}q_F\left(c_x^2 - \frac{3}{2}\right)\right] \tag{19}$$

$$c_x\frac{\partial Y_F}{\partial x} + \delta Y_F = \delta\left[\tau_F + \frac{4}{15}q_F c_x\right] \tag{20}$$

In Eqs. (19) and (20), $x \in [-1/2, 1/2]$ is the space coordinate, c_x is the x – component of the molecular velocity and $\rho_F(x)$, $\tau_F(x)$, $q_F(x)$ are the perturbed macroscopic velocity, temperature and heat flux distributions written as

$$\rho_F(x) = \frac{1}{\sqrt{\pi}}\int_{-\infty}^{\infty}\Phi_F(x, c_x)\exp(-c_x^2)dc_x \tag{21}$$

$$\tau_F(x) = \frac{1}{3\sqrt{\pi}}\int_{-\infty}^{\infty}\left[2Y_F(x, c_x) + \Phi_F(x, c_x)(2c_x^2 - 1)\right]\exp(-c_x^2)dc_x \tag{22}$$

$$Q = q_F(x) = \frac{1}{\sqrt{\pi}}\int_{-\infty}^{\infty}\left[Y_F(x, c_x) + \Phi_F(x, c_x)\left(c_x^2 - \frac{3}{2}\right)\right]c_x\exp(-c_x^2)dc_x \tag{23}$$

The heat flux Q is the main output quantity and is constant across the plates.

At $x = \mp 1/2$, the CL boundary conditions read as:

$$\Phi_F(\mp 1/2, c_x \gtrless 0) = \mp\frac{\alpha_n}{2}(1 - c_x^2) + \frac{2}{\alpha_n}\int_{c'_x \lessgtr 0}|c'_x|\exp\left(-\frac{c'^2_x + (1-\alpha_n)c_x^2}{\alpha_n}\right) \times I_0\left(\frac{2\sqrt{1-\alpha_n}c_x c'_x}{\alpha_n}\right)\Phi_F(\mp 1/2, c'_x \lessgtr 0)dc'_x \tag{24}$$

$$Y_F(\mp 1/2, c_x \gtrless 0) = \mp\frac{\alpha_t(2-\alpha_t)}{2} + \frac{2(1-\alpha_t)^2}{\alpha_n}\int_{c'_x \lessgtr 0}|c'_x|\exp\left(-\frac{c'^2_x + (1-\alpha_n)c_x^2}{\alpha_n}\right) \times I_0\left(\frac{2\sqrt{1-\alpha_n}c_x c'_x}{\alpha_n}\right)Y_F(\mp 1/2, c'_x \lessgtr 0)dc'_x \tag{25}$$

Each problem has been solved for many values of α_t and α_n in the whole range of δ in order to provide an adequate dense database of the corresponding main output quantity to be employed in the MC

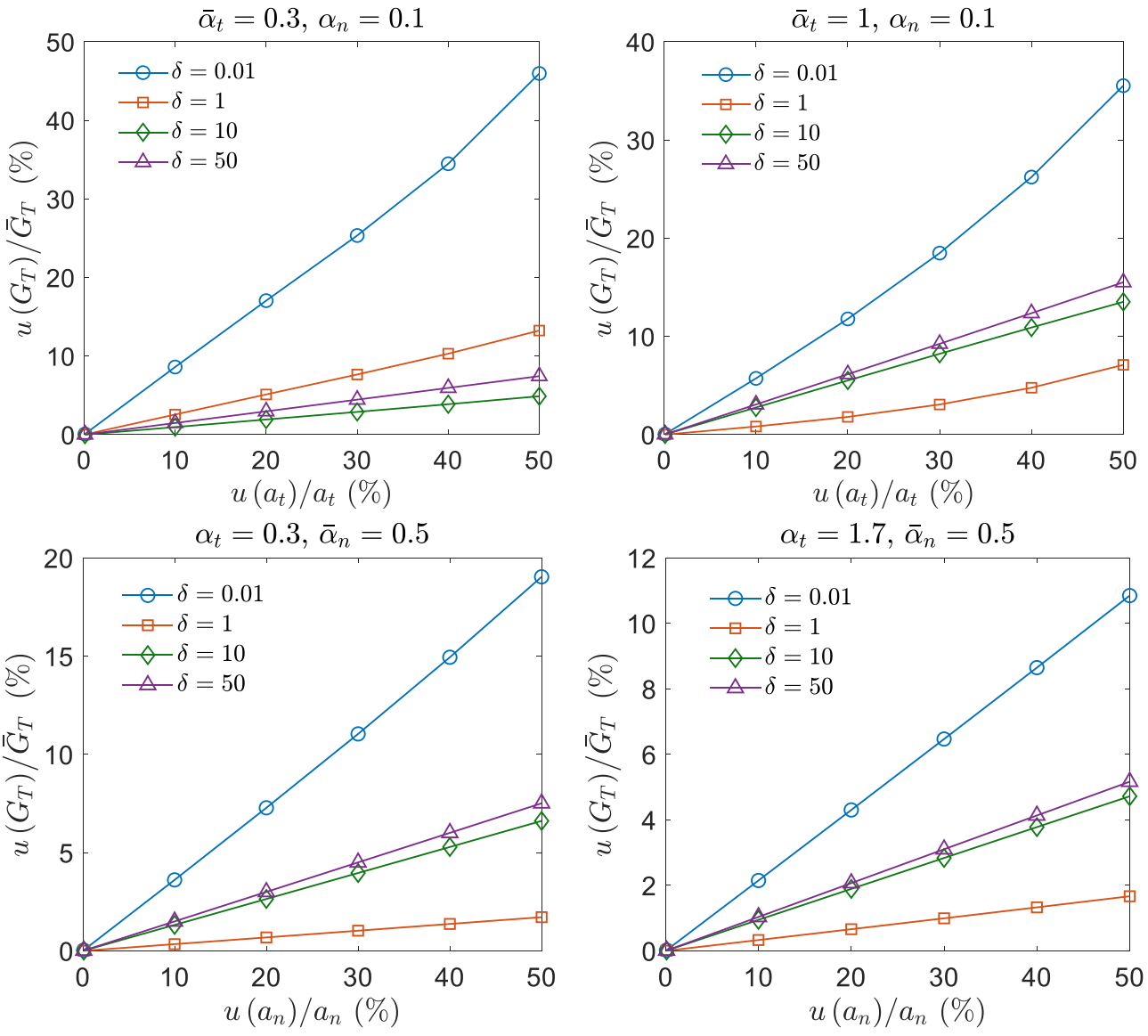

Fig. 8. Thermal creep flow – Uncertainty of reduced flow rate $u(G_T)/\overline{G}_T$ vs $u(\alpha_t)/\overline{\alpha}_t$, with $\overline{\alpha}_t = [0.3, 1]$ and $\alpha_n = [0.1]$ (up) and $u(\alpha_n)/\overline{\alpha}_n$, with $\overline{\alpha}_n = [0.5]$ and $\alpha_t = [0.3, 1.7]$ (down) for $\delta = [10^{-2},\ 1,\ 10,\ 50]$.

uncertainty propagation analysis performed in Section 3. The databases consist of the flow rates G_P and G_T for the Poiseuille and thermal creep flows respectively, the shear stress Π for the Couette flow and the heat flux Q for the Fourier flow and are provided in digital form in the supplementary material.

3. Uncertainty analysis via the Monte Carlo method

The objective is to formally analyze the effect of the CL ACs on the main output quantities of the considered prototype problems in the whole range of gas rarefaction. This may be numerically fulfilled by introducing, in each problem, some uncertainties in the ACs, which are treated as input quantities and compute the corresponding deduced uncertainty of the main output quantity. It is expected the sensitivity of the output quantity on the ACs to be stronger, when, for a given input uncertainty, the uncertainty of the output quantity is large.

Among other methods, the stochastic Monte Carlo (MC) method has been chosen as the most suitable for the present work, due to its versatility to provide probabilistic insights in complex problems such as the solution of differential and integrodifferential equations, where analytical solutions are not available, without requiring model assumptions [64,68]. The same approach has been applied in [55] to investigate the importance of uncertainties of other input data, such as pressure, temperature, radius, and Maxwell AC on the flow rates of the Poiseuille and thermal creep flows and it also employed in the present work.

A discussion of the implemented uncertainty analysis is provided. The ACs α_t and α_n can be represented as $\alpha_j = \overline{\alpha}_j \pm u(\alpha_j)$, with $j = [t, n]$, where $\overline{\alpha}_j$ denotes the nominal (or mean) value and $u(\alpha_j)$ is the associated uncertainty introduced in the AC α_j, The main output quantity in each problem can be represented as $y = \overline{y} \pm u(y)$, with $y = [G_P, G_T, \gamma, \Pi, Q]$, where $\overline{y}$ is the mean value and $u(y)$ is the computed output uncertainty.

A large number of trials N_t is performed in each problem. In each trial a value of one input quantity, either α_t or α_n is sampled, based on a specific distribution, from the interval $a_j \in [\overline{\alpha}_j - u(\alpha_j), \overline{\alpha}_j + u(\alpha_j)]$ and the corresponding value of the output quantity y_i, $i = 1, 2, \ldots, N_t$, is obtained based on the computational model. When one of the ACs is subject to uncertainty, the uncertainty of the second one is assumed to be zero. This way the effect of each AC is separately obtained.

By performing the required number of trials, the mean value of the

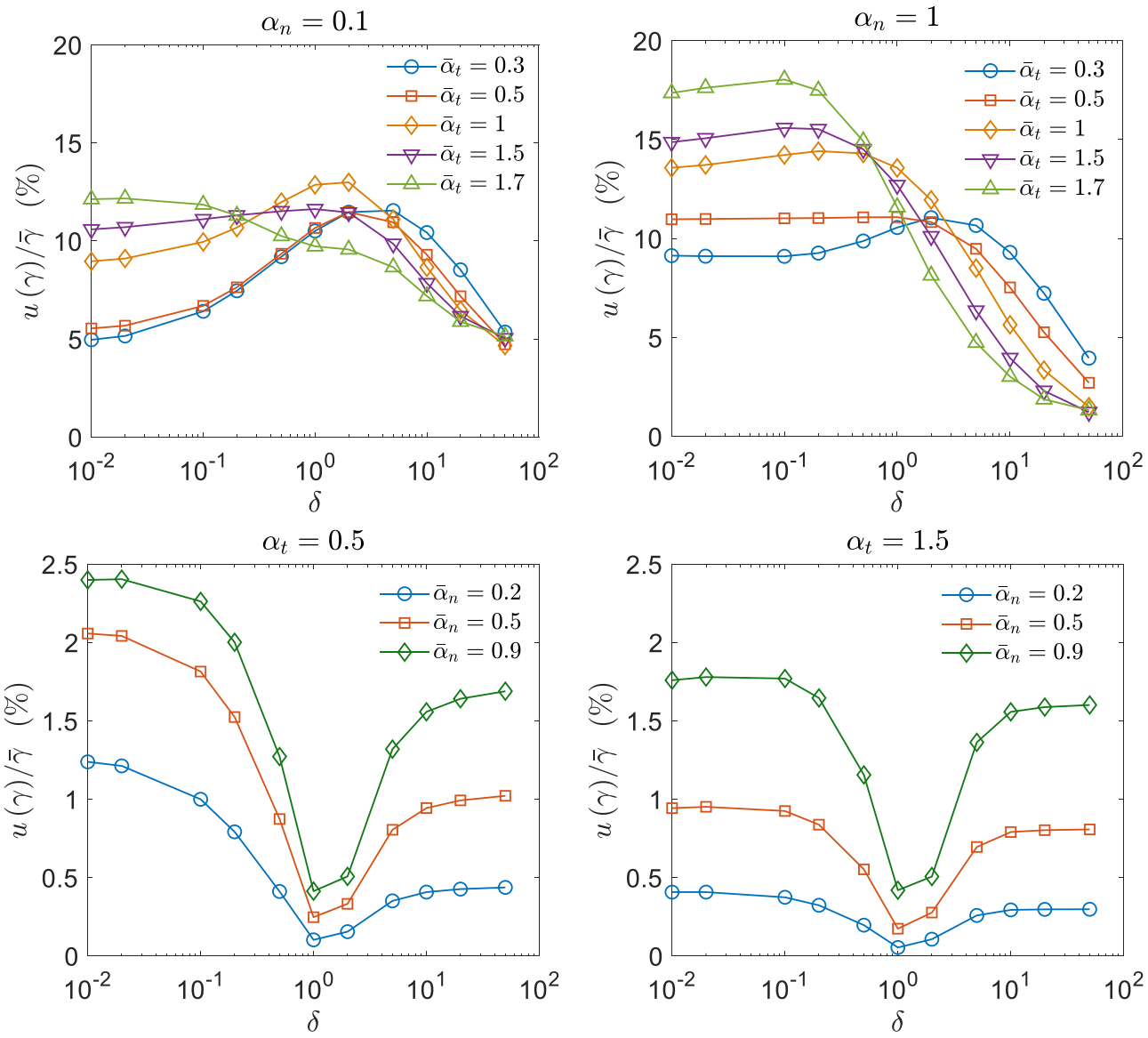

Fig. 9. TPD flow – Uncertainty of exponent $u(\gamma)/\overline{\gamma}$ vs δ for input uncertainty $u(\alpha_t)/\overline{\alpha}_t = 10\%$, with $\overline{\alpha}_t = [0.3, 0.5,\ 1,\ 1.5, 1.7]$, $\alpha_n = [0.1,\ 1]$ (up) and $u(\alpha_n)/\overline{\alpha}_n = 10\%$, with $\overline{\alpha}_n = [0.2,\ 0.5, 0.9]$, $\alpha_t = [0.5,\ 1.5]$ (down).

output quantities $\overline{y}$ is calculated as

$$\overline{y} = \frac{1}{N_t}\sum_{i=1}^{N_t} y_i \tag{26}$$

while the associated uncertainty $u(y)$ is calculated as

$$u(y) = k_p \sigma_y \tag{27}$$

where σ_y is the standard deviation, given by

$$\sigma_y = \sqrt{\frac{1}{N_t - 1}\sum_{i=1}^{N_t} (y_i - \overline{y})^2} \tag{28}$$

and k_p is the specified coverage factor ($k_p = 2$ and $k_p = 3$ correspond to 95 % and 99 % coverage intervals respectively). The uncertainties in the input and output quantities, provided in the next section, are always reported as relative uncertainties on a percentage basis defined as

$$\frac{u(\alpha_j)}{\overline{\alpha}_j} \times 100\% \text{ and } \frac{u(y)}{\overline{y}} \times 100\% \tag{29}$$

In the present work, $N_t = 1000$ trials have been conducted and the input quantities are sampled from a uniform distribution as $\alpha_j = \overline{\alpha}_j + u(\alpha_j)(1 - 2R_f), j = [t,n]$, where R_f is a random number between 0 and 1. The actual distribution of the input quantities is not known, and the uniform distribution is the appropriate choice based on the principle of maximum entropy, as the least informative distribution. Then, by solving the governing equations, with the associated boundary conditions for each problem under consideration, the corresponding distribution function of the main output quantity $y = [G_P, G_T, \gamma, \Pi, Q]$ is obtained. Finally, the distribution function of each main output quantity is used to calculate the respective uncertainty. It turns out that the distribution function of the output quantity y, always maintains a close resemblance to a uniform distribution in all cases examined. Therefore, in all cases, results are provided only for the output uncertainties and not for the output distributions.

4. Results and discussion

Results for the Poiseuille, thermal creep, TPD, Couette and Fourier flows are presented. In each of the five protype problems considered, the

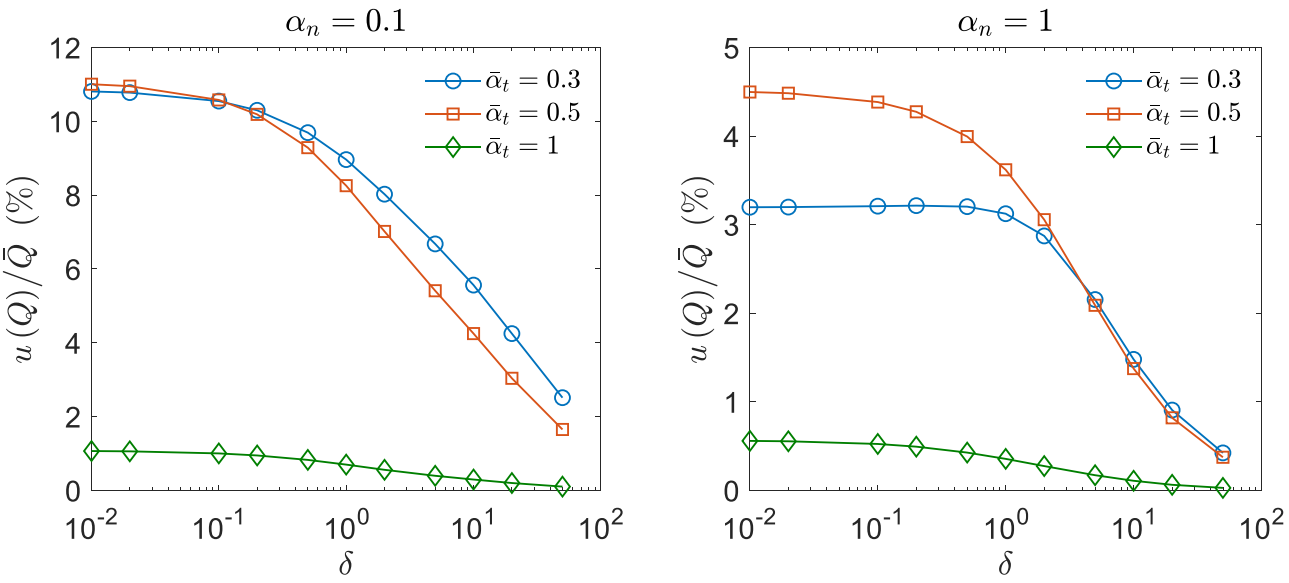

Fig. 10. Fourier flow – Uncertainty of dimensionless heat flux $u(Q)/\overline{Q}$ vs δ for input uncertainty, with $u(\alpha_t)/\overline{\alpha}_t = 10\%$ and $\alpha_n = [0.1,\ 1]$.

uncertainties of the main output quantity, namely, $\frac{u(y)}{\bar{y}} = \left[\frac{u(G_P)}{\overline{G}_P}, \frac{u(G_T)}{\overline{G}_T}, \frac{u(\gamma)}{\bar{\gamma}}, \frac{u(\Pi)}{\overline{\Pi}}, \frac{u(Q)}{\overline{Q}}\right]$ is provided in terms of the input uncertainties $\frac{u(\alpha_t)}{\overline{\alpha}_t}$ and $\frac{u(\alpha_n)}{\overline{\alpha}_n}$ in a wide range of the gas rarefaction parameter $\delta \in [0, 50]$ (from the free molecular limit to the slip regime). In most cases the input uncertainty of the ACs has been set equal to 10 %, while input uncertainties up to 50 % have been also examined. Also, in all reported output uncertainties the coverage factor is $k_p = k_{95} = 2$ and corresponds to 95 % coverage interval, which slightly overestimates the uncertainty in the case of a uniform distribution.

In each problem, the effect of the ACs is discussed and the flow setups, as well as the gas rarefaction regimes, where the extraction of the AC is facilitated or hindered are pointed out.

4.1. Poiseuille and couette flows

In the Poiseuille flow, the uncertainty of the reduced flow rate $u(G_P)/\overline{G}_P$ versus δ is shown in Figs. 1 and 2, with regard to the input uncertainties $u(\alpha_t)/\overline{\alpha}_t$ and $u(\alpha_n)/\overline{\alpha}_n$ respectively. In both cases the input uncertainty is set equal to 10 %. In Fig. 1, the nominal values of $\overline{\alpha}_t = [0.3, 0.5,\ 1,\ 1.5, 1.7]$ are examined, covering the range of $\alpha_t \in [0,\ 2]$, while $\alpha_n = 1$ is kept constant. For $\delta \leq 3$, the output uncertainties are larger than the input ones. They are about 15 %, when $\alpha_t \leq 1$ and they further increase when $\alpha_t > 1$ (backscattering). On the contrary, for $\delta > 3$ they are less than the input ones, but they remain above 5 %, even up to $\delta = 10$, particularly when $\alpha_t < 1$. Similar results have been obtained for $\alpha_n < 1$. In Fig. 2, the nominal values of $\overline{\alpha}_n = [0.2,\ 0.5,\ 0.9]$ are examined, covering the range of $\alpha_n \in [0, 1]$. To have a complete view of the effect of α_n in the whole range of α_t, results are provided for $\alpha_t = [0.3, 0.5,\ 1.5, 1.7]$. Always, the output uncertainty is very small, clearly verifying that the reduced flow rate G_P is practically independent of α_n. Since in the Poiseuille flow, α_t is the only AC affecting the flow, in Fig. 3, $u(G_P)/\overline{G}_P$ versus $u(\alpha_t)/\overline{\alpha}_t$, varying from zero up to 50 %, with $\overline{\alpha}_t = [0.3,\ 1]$ and $\alpha_n = 1$, is plotted for representative values of $\delta \in [0, 50]$. It is seen that the output uncertainty grows almost linearly with the input one and this is valid for any value of α_t.

The presented results justify, to certain extend, the straightforward and accurate estimation of the CL tangential momentum AC, even in the slip regime, via experimental work in purely pressure driven flows [13, 49].

In the Couette flow, the main output quantity is the dimensionless shear stress Π and its computed uncertainty versus δ is shown in Figs. 4 and 5, with regard to the input uncertainties $u(\alpha_t)/\overline{\alpha}_t$ and $u(\alpha_n)/\overline{\alpha}_n$ respectively. Both input uncertainties are 10%.

In Fig. 4, $u(\Pi)/\overline{\Pi}$is plotted for nominal values of $\overline{\alpha}_t = [0.3, 0.5,\ 1,\ 1.5, 1.7]$ with $\alpha_n = 1$. For $\delta < 1$, the output uncertainty is much larger than the input one, particularly in the free molecular regime, where the dependency of the shear stress on α_t is even stronger than the corresponding one of G_P in the Poiseuille flow. For $\delta = 1$, the output uncertainty is about the same as the input one and then, as δ increases it further reduces. Similar results have been obtained for $\alpha_n < 1$. In Fig. 5, $u(\Pi)/\overline{\Pi}$ is plotted for nominal values of $\overline{\alpha}_n = [0.2,\ 0.5,\ 0.9]$ and various values of α_t. In all cases, the output uncertainty has a peak close to $\delta = 1$, but the major issue is that it always remains less than 1 %. Thus, the shear stress in the Couette flow depends only on α_t and is practically independent of α_n.

Surely, experimental work in plane or cylindrical Couette-type flow setups, under high gas rarefaction conditions, is expected to deduce very accurate estimates of the tangential momentum AC. Such work has been reported mainly for the Maxwell tangential momentum AC [69,70].

4.2. Thermal creep and TPD flows

In the thermal creep flow, the uncertainty of the reduced flow rate $u(G_T)/\overline{G}_T$ versus δ is shown in Figs. 6 and 7, with regard to the input uncertainties $u(\alpha_t)/\overline{\alpha}_t = 10\%$ and $u(\alpha_n)/\overline{\alpha}_n = 10\%$ respectively. In Fig. 6, the nominal values of the tangential momentum AC are $\overline{\alpha}_t = [0.3,\ 0.5,\ 1,\ 1.5, 1.7]$ for representative values of $\alpha_n = [0.1,\ 1]$, while in Fig. 7, the nominal values of the normal energy AC are $\overline{\alpha}_n = [0.2,\ 0.5, 0.9]$ for representative values of$\alpha_t = [0.3, 0.5,\ 1.5, 1.7]$.

In Fig. 6, it is seen that the output uncertainty $u(G_T)/\overline{G}_T$ remains always smaller than the input one ($u(\alpha_t)/\overline{\alpha}_t = 10\%$), except in the case of strong back scattering ($\alpha_t \geq 1.5$), where for small values of δ reaches about 25 %. Also, as α_t approaches one, either from below or above, as well as when α_n increases, the effect of α_t on the flow rate (i.e. the uncertainties of G_T) decreases (for $\alpha_t = \alpha_n = 1$ the uncertainty becomes negligible), while in general, for $\delta \geq 2$ the output uncertainties are small. Comparing these results with the corresponding ones in Fig. 1, it is evident that G_P depends on α_t stronger than G_T and therefore it easier to extract α_t based on the Poiseuille rather than on the thermal creep flow.

In Fig. 7, the sensitivity of the thermal creep flow rate on the normal

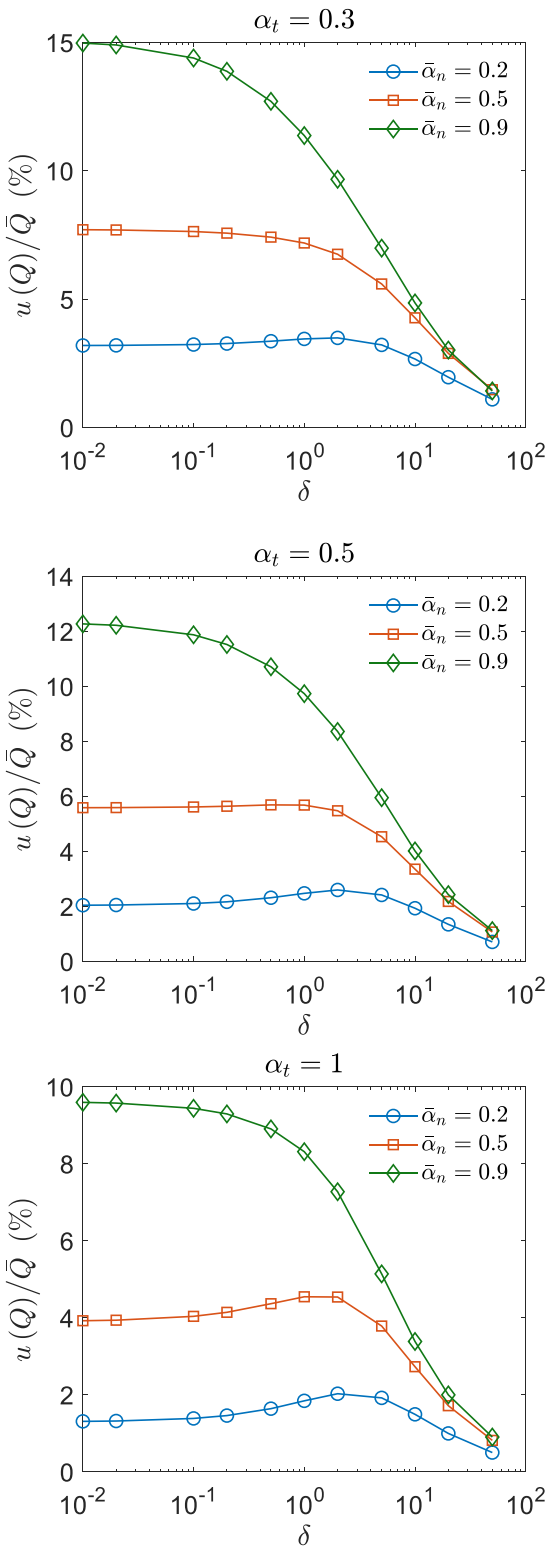

Fig. 11. Fourier flow – Uncertainty of dimensionless heat flux $u(Q)/\overline{Q}$ vs δ for input uncertainty $u(\alpha_n)/\overline{\alpha}_n = 10\%$, with $\overline{\alpha}_n = [0.2,\ 0.5, 0.9]$ and $\alpha_t = [0.3,\ 0.5,\ 1]$.

energy AC is shown. For all nominal values of α_n, the output uncertainties $u(G_T)/\overline{G}_T$ are significantly smaller than the input ones $u(\alpha_n)/\overline{\alpha}_n = 10\%$. Comparing these results with the corresponding ones in Fig. 2, it is stated that G_T depends on α_n much stronger than G_P, but still the dependency is not strong enough to permit a straightforward extraction of α_n, unless the experimental work is performed under high rarefied conditions and the experimental uncertainties are reduced below the ones presented in Fig. 7 (less than 4 %), which of course is not easily achieved. In general, the uncertainties increase with α_n but they always remain small. Also, when $\delta = 1 - 2$, the sensitivity of G_T on α_n almost diminishes. Comparing the effect of α_t and α_n on G_T, in Figs. 6 and 7, it may be stated that the former one is more pronounced at $\delta \leq 1$, while their effect remains small at $\delta \geq 1$.

In Fig. 8, the output uncertainty versus the input ones, varying from zero up to 50 %, is plotted for indicative values of the ACs and representative gas rarefaction parameters $\delta \in [0,50]$. Similar to the Poiseuille flow, the output uncertainty in the thermal creep flow, grows almost linearly with the input one and this is true for any value of α_t and α_n. Based on the observed linear behavior, the output uncertainties may also be calculated for different values of the input ones.

In the TPD flow, the output uncertainty $u(\gamma)/\overline{\gamma}$ remains relatively small with regard to the input ones, as in the case of the thermal creep flow, and therefore, only few indicative results are presented. In Fig. 9, $u(\gamma)/\overline{\gamma}$ is plotted versus δ for input uncertainty $u(\alpha_t)/\overline{\alpha}_t = 10\%$ (top) and $u(\alpha_n)/\overline{\alpha}_n = 10\%$ (bottom). Compared to thermal creep flow (Figs. 7 and 8), there is a quantitative difference in the tangential momentum AC, where, its effect becomes more dominant as α_t approaches one (either from below or above), with the output uncertainty obtaining values around 15 % at $\alpha_t = 1$, when $\delta \leq 1$. Also, the effect of α_t on the exponent γ increases with α_n and, in general, it remains significant in a wider range of δ. This behavior is opposite to the one observed in the thermal creep flow. Unfortunately, the behavior of the exponent γ with regard to α_n is almost quantitatively identical to the one observed in thermal creep flow (compare Fig. 9 (bottom) with Fig. 8). Thus, taking into consideration that temperature driven flows should be useful in the estimation of the CL normal energy AC, it is deduced that the employment of the TPD, instead of the thermal creep flow, is not expected to be particularly useful, unless of course the involved experimental uncertainties are significantly reduced.

Overall, it is seen that the employment of the thermal creep or TPD flows, does not facilitate the extraction α_n, since the dependency of the reduced flow rate and exponent respectively on α_n is relatively weak, in a wide range of gas rarefaction. The whole effort becomes even harder when the work is conducted in the late transition and slip regimes, where indicatively, the experimental uncertainties must be below 4 % in order to obtain estimates of α_n with reliability of 10%.

4.3. Fourier flow

In the Fourier flow, the main output quantity is the dimensionless heat flux Q and its computed uncertainty versus δ is shown in Figs. 10 and 11, with regard to the input uncertainties $u(\alpha_t)/\overline{\alpha}_t$ and $u(\alpha_n)/\overline{\alpha}_n$ respectively. Both input uncertainties are 10%. In the Fourier flow the heat flux is symmetric about $\alpha_t = 1$, independent of the value of α_n and therefore, the output uncertainties $u(Q)/\overline{Q}$ are presented only for $\alpha_t \in [0,\ 1]$.

To demonstrate the effect of α_t, in Fig. 10, $u(Q)/\overline{Q}$ is plotted for nominal values of $\overline{\alpha}_t = [0.3, 0.5,\ 1]$ with $\alpha_n = [0.1,\ 1]$. The output uncertainties increase as δ decreases (this is well expected), as well as when α_t and α_n decrease, i.e., as the tangential momentum and normal energy accommodations become more specular. In general, the output uncertainty $u(Q)/\overline{Q}$ is about the same or smaller than the input one $u(\alpha_t)/\overline{\alpha}_t = 10\%$ and therefore, Poiseuille or Couette flow setups are more suitable compared to Fourier flow setups, for the extraction of α_t.

To demonstrate the effect of α_n, in Fig. 11, $u(Q)/\overline{Q}$ is plotted for nominal values of $\overline{\alpha}_n = [0.2,\ 0.5, 0.9]$ with $\alpha_t = [0.3, 0.5,\ 1]$. The output uncertainties increase as δ decreases, as well as when α_t decreases and when α_n increases. The output uncertainties $u(Q)/\overline{Q}$ remain in the same range as the ones in α_t surpassing in some cases the input one $u(\alpha_n)/\overline{\alpha}_n = 10\%$. Comparing with the corresponding results in Figs. 7 and 11, it is

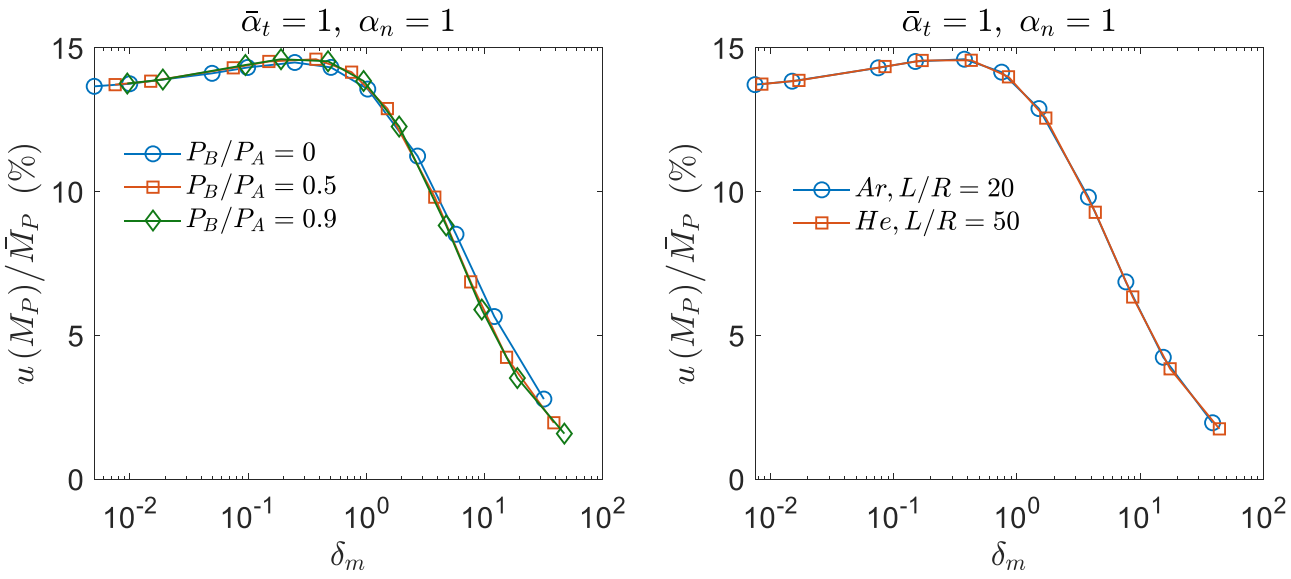

Fig. 12. Poiseuille flow – Uncertainty of mass flow rate $u(M_P)/\overline{M}_P$ vs δ_m for input uncertainty $u(\alpha_t)/\overline{\alpha}_t = 10\%$, with $\overline{\alpha}_t = 1$ and $\alpha_n = 1$.

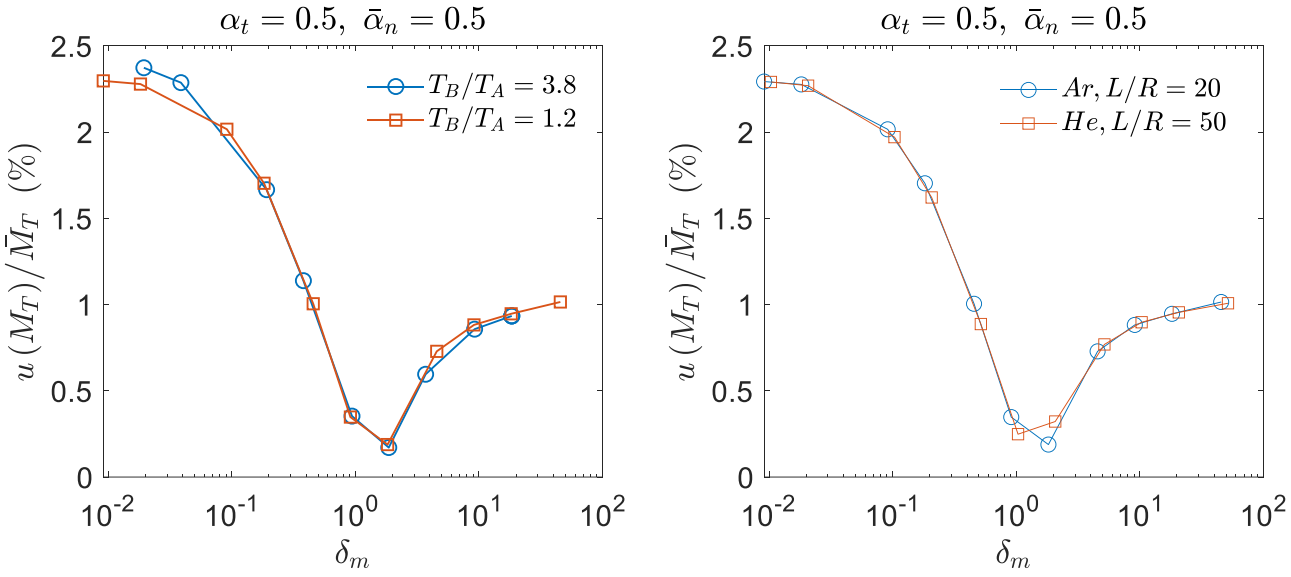

Fig. 13. Thermal creep flow – Uncertainty of mass flow rate $u(M_T)/\overline{M}_T$ vs δ_m for input uncertainty $u(\alpha_n)/\overline{\alpha}_n = 10\%$, with $\overline{\alpha}_n = 0.5$ and $\alpha_t = 0.5$.

evident that the heat flux Q is more sensitive than the flow rate G_T to α_n. Therefore, the Fourier heat transfer setup may be more suitable than the thermal creep flow to extract the normal energy AC, particularly in the transition and free molecular regimes, provided that the tangential momentum AC has been already accordingly fixed via some Poiseuille or Couette flow configuration. Furthermore, by varying the input uncertainties $u(\alpha_t)/\overline{\alpha}_t$ and $u(\alpha_n)/\overline{\alpha}_n$ from zero up to 50 %, it is verified that the output uncertainty, as in the case of the other flow setups increases linearly with respect to the input ones (not shown here). The above remarks are expected to remain valid also in the case of Fourier flow between concentric cylinders.

4.4. *Effect of the CL accommodation coefficients on the dimensional main output quantities*

So far, the analysis has been performed in dimensionless form. The sensitivity of the main dimensionless output quantity of each problem, namely $y = [G_P, G_T, \gamma, \Pi, Q]$, on α_t and α_n, in the whole range of δ, has been examined, by assuming driving forces of infinitesimal small magnitude. In order to investigate the effect of small but finite magnitude driving forces, as well as of other parameters, such as problem geometry and working gas, on the reported results, in this section, the sensitivity of the associated main dimensional output quantity of each problem on α_t and α_n, for indicative flow setups, is considered. Also, this task facilitates the implementation of the present analysis in future experimental work.

For the Poiseuille, thermal creep and TPD flows, consider the fully-developed gas flow through a long capillary of radius $R = 0.485$mm and length L, with $L/R = [20, 50]$, connecting two containers (A and B) maintained at some pressures P_i and temperatures T_i, with $i = A,B$. The reference pressure and temperature are the ones of container A, while the working gases are helium (He) and argon (Ar).

In the Poiseuille flow, the reference pressure ranges as $P_A = [0.16 - 800]$Pa and the flow is due to the pressure ratios $P_B/P_A = [0, 0.5, 0.9]$ ($T_A = T_B$). The main dimensional output quantity is the mass flow rate, given by [12,71]

$$M_P = \frac{\pi R^3 G_P^*}{v_0}\frac{P_B - P_A}{L} \tag{30}$$

where $G_P^* = \frac{1}{\delta_B - \delta_A}\int_{\delta_A}^{\delta_B} G_P d\delta$, with δ_A and δ_B denoting the gas rarefaction parameters in containers A and B. In Fig. 12, the uncertainties $u(M_P)/\overline{M}_P$ versus the average gas rarefaction parameter $\delta_m = (\delta_A + \delta_B)/2$ is plotted for input uncertainties $u(\alpha_t)/\overline{\alpha}_t = 10\%$, with $\overline{\alpha}_t = 1$ and $\alpha_n = 1$ for various pressure and length to radius ratios and for He and Ar. In all cases, the deduced uncertainties almost coincide to each other and are in excellent agreement with the corresponding ones in Fig. 1, clearly indicating that the effect of the magnitude for the driving force, the capillary geometry and the working gas on the sensitivity of the Poiseuille flow rate on α_t is negligible.

In the thermal creep flow, the reference temperature is $T_A = 297.5$K and the flow is due to the temperature ratios $T_B/T_A = [1.2,\ 3.8]$, assuming linear temperature variation along the capillary, with $P_A = P_B = [0.16 - 800]$Pa. The main dimensional output quantity is the mass flow rate, given by

$$M_T = -\frac{\pi R^3}{v_0(z)}\frac{dP(z)}{dz}G_P(\delta, \alpha_t, a_n) + \frac{\pi R^3}{v_0(z)}\frac{P(z)}{T(z)}\frac{dT(z)}{dz}G_T(\delta, \alpha_t, a_n) \tag{31}$$

Following a well-known procedure, M_T as well as the pressure and pressure gradient distributions along the capillary are obtained [65,72,73]. In Fig. 13, the uncertainties $u(M_T)/\overline{M}_T$ versus the average gas rarefaction parameter $\delta_m = (\delta_A + \delta_B)/2$ is plotted for input uncertainties $u(\alpha_n)/\overline{\alpha}_n = 10\%$, with $\overline{\alpha}_n = [\,0.5]$ and $\alpha_t = [0.5]$ for two temperature and length to radius ratios and for He and Ar. Again, the deduced uncertainties are in excellent agreement and there is very good resemblance with the corresponding results in Fig. 7. Thus, the effect of the magnitude for the temperature difference, the capillary geometry and the working gas on the sensitivity of the thermal creep flow rate on α_n is negligible. In the TPD flow, the main output quantity is the pressure ratio P_B/P_A and is obtained by Eq. (31), with $M_T = 0$. Similarly, the computed uncertainties (not shown here) are very close to the ones reported in Fig. 9.

In the plane Couette and Fourier flows, the dimensional shear stress $\widehat{\Pi}$ and heat flux $\widehat{Q}$ are directly related with the dimensionless ones, as $\widehat{\Pi} = \Pi P U_w/v_0$ and $\widehat{Q} = QPv_0\Delta T/T_m$, where P is some reference pressure, U_w is the wall velocity, $\Delta T = T_1 - T_2$ is the temperature difference between the temperature of the two plates and T_m is the reference average temperature. Thus, it is obvious that the uncertainties of the dimensional shear stress and heat flux should always accordingly align with the corresponding dimensionless ones in Figs. 4–5 for the Couette flow and Figs. 10–11 for the Fourier flow respectively and are independent of the distance between the plates and the working gas. They are also independent of the ratios U_w/v_0 and T_1/T_2, provided that they are adequately small to permit the implementation of the linear S kinetic model.

Overall, it is stated that the results in Sections 4.1, 4.2 and 4.3 are valid in a wide range of operating conditions and geometry characteristics for any monatomic gas subject to the main assumptions of fully developed flow and linear heat transfer.

5. Concluding remarks

In the present work the objective is to quantitatively determine the effect of the CL ACs on main output quantities of various representative type flow and heat transfer configurations, in the whole range of gas rarefaction. It is fulfilled by performing a formal and detailed sensitivity propagation analysis via the Monte Carlo method. The cylindrical Poiseuille, thermal creep and TPD flows, as well as the plane Couette and Fourier flows have been examined. In each problem some uncertainty is introduced in the tangential momentum (α_t) or normal energy (α_n) AC and the associated uncertainty of the main output quantity is stochastically computed in the whole range of the gas rarefaction parameter δ. The flow setups and the rarefaction regimes with the larger output uncertainties are the most suitable ones for the estimations of the ACs, since larger modeling and experimental errors may be acceptable.

It has been found that the flow rate and the shear stress of the Poiseuille and Couette flows respectively are strongly affected by α_t. More specifically, in moderate and high gas rarefaction the uncertainty of the output quantities may be several times higher than the input uncertainty of α_t. On the contrary, the output quantities are not affected, at all, by α_n. Either of these flows is very suitable for the accurate estimation of α_t, allowing relatively large uncertainties in measurements and computations. Furthermore, it has been found that the flow rate and the exponent in the thermal creep and TPD (zero net mass flow) flows respectively, are affected by both CL coefficients, but in a rather weak manner. Considering that α_t has been already fixed, here, we are mostly interesting on the sensitivity of the output quantities with respect to α_n, which unfortunately turns out to be very small. Indicatively, for an input uncertainty of 10 %, the output uncertainties in either the thermal creep or TPD flows, are less than 4 % in the whole range of δ, which clearly implies that the estimation of α_n within 10 % requires uncertainties <4 % in measurements and computations. Finally, in the Fourier flow it has been found that the heat flux is affected, in a rather moderate manner by both coefficients, particularly for $\delta \leq 1$, where for example, an input uncertainty of 10 % in α_n, yields a heat flux with about the same uncertainty. Thus, there is a larger upper margin for numerical and experimental uncertainties. Comparing the corresponding results between the thermal creep, TPD and Fourier flows it is deduced that for the reliable estimation of the CL normal energy AC, it is more suitable to combine the Poiseuille (or Couette) and Fourier configurations, rather than, as it is commonly done, the Poiseuille and thermal creep (or TPD) ones.

The present analysis has been performed in dimensionless form, assuming infinitesimal small driving forces and therefore, the output dimensionless quantities depend only on the ACs and δ. It has been shown however, that the presented results remain valid even in the case of small but finite pressure and temperature differences and are independent of the working gas and geometrical characteristics. Thus, the presented behavior of the effect of the CL ACs is general and may be applied in the characterization of gas-surface interaction in prototype setups, as well as in more realistic and complex configurations in microfluidics and vacuum technology. Furthermore, the present sensitivity analysis may be extended in polyatomic gases based on the Cercignani-Lampis-Lord kernel [31], as well as in other gas-surface scattering kernels with molecular velocity dependent ACs [61,62].

CRediT authorship contribution statement

Giorgos Tatsios: Writing – review & editing, Validation, Software, Methodology, Conceptualization. **Thanasis Basdanis:** Writing – review & editing, Writing – original draft, Visualization, Validation, Software, Methodology, Investigation, Formal analysis, Data curation, Conceptualization. **Dimitris Valougeorgis:** Writing – review & editing, Writing – original draft, Supervision, Project administration, Methodology, Funding acquisition, Conceptualization.

Declaration of Competing Interest

The authors declare that they have no known competing financial interests or personal relationships that could have appeared to influence the work reported in this paper.

Data availability

The data that support the findings of this study are available within the article and its supplementary material.

Acknowledgements

This work has been carried out within the framework of the EUROfusion Consortium, funded by the European Union via the Euratom Research and Training Programme (Grand Agreement No 101052200 - EUROfusion), as well as the National Program of Controlled Thermonuclear Fusion. Views and opinions expressed are however those of the author(s) only and do not necessarily reflect those of the European Union or the European Commission. Neither the European Union nor the European Commission can be held responsible for them. This work was supported by computational time granted from the EUROfusion HPC Marconi Fusion and the National Infrastructures for Research and Technology S.A. (GRNET S.A.) in the National HPC facility ARIS.

Appendix A. Supporting information

Supplementary data associated with this article can be found in the online version at doi:10.1016/j.euromechflu.2024.05.003.

References

[1] S. Colin, Heat Transfer and Fluid Flow in Minichannels and Microchannels, Elsevier, 2006.
[2] C. Shen, Rarefied Gas Dynamics: Fundamentals, Simulations and Micro Flows, Springer, Berlin; New York, NY, 2005.
[3] K. Jousten, Handbook of Vacuum Technology, John Wiley & Sons, 2016.
[4] N. Vasileiadis, G. Tatsios, S. Misdanitis, D. Valougeorgis, Modeling of complex gas distribution systems operating under any vacuum conditions: simulations of the ITER divertor pumping system, Fusion Eng. Des. 103 (2016) 125–135.
[5] S. Naris, N. Vasileiadis, D. Valougeorgis, A.S. Hashad, W. Sabuga, Computation of the effective area and associated uncertainties of non-rotating piston gauges FPG and FRS, Metrologia 56 (2019) 015004.
[6] K. Breuer, Lubrication in MEMS, in: M. Gad-el-Hak (Ed.), The MEMS Handbook, CRC Press, 2001.
[7] L. Wu, M.T. Ho, L. Germanou, X.-J. Gu, C. Liu, K. Xu, Y. Zhang, On the apparent permeability of porous media in rarefied gas flows, J. Fluid Mech. 822 (2017) 398–417.
[8] M.T. Ho, L. Zhu, L. Wu, P. Wang, Z. Guo, Z.-H. Li, Y. Zhang, A multi-level parallel solver for rarefied gas flows in porous media, Comput. Phys. Commun. 234 (2019) 14–25.
[9] J. Chen, H. Zhou, Rarefied gas effect in hypersonic shear flows, Acta Mech. Sin. 37 (2021) 2–17.
[10] A. Alexeenko, D. Levin, S. Gimelshein, M. Ivanov, A. Ketsdever, Numerical and Experimental Study of Orifice Flow in the Transitional Regime. in: 35th AIAA Thermophysics Conference, American Institute of Aeronautics and Astronautics, Anaheim,CA,U.S.A., 2001.
[11] C. Cercignani, The Boltzmann Equation and Its Applications, Springer New York, New York, NY, 1988.
[12] F. Sharipov, V. Seleznev, Data on internal rarefied gas flows, J. Phys. Chem. Ref. Data 27 (1998) 657–706.
[13] F. Sharipov, Data on the velocity slip and temperature jump on a gas-solid interface, J. Phys. Chem. Ref. Data 40 (2011) 023101.
[14] B.-Y. Cao, J. Sun, M. Chen, Z.-Y. Guo, Molecular momentum transport at fluid-solid interfaces in MEMS/NEMS: a review, IJMS 10 (2009) 4638–4706.
[15] T. Acharya, J. Falgoust, I. Schoegl, M.J. Martin, Measurement of variation of momentum accommodation coefficients with molecular mass and structure, J. Thermophys. Heat. Transf. 33 (2019) 773–778.
[16] S. Mohammad Nejad, S. Nedea, A. Frijns, D. Smeulders, The influence of gas–wall and gas–gas interactions on the accommodation coefficients for rarefied gases: a molecular dynamics study, Micromachines 11 (2020) 319.
[17] S. Mohammad Nejad, E. Iype, S. Nedea, A. Frijns, D. Smeulders, Modeling rarefied gas-solid surface interactions for Couette flow with different wall temperatures using an unsupervised machine learning technique, Phys. Rev. E 104 (2021) 015309.
[18] J.C. Maxwell VII, On stresses in rarified gases arising from inequalities of temperature, Philos. Trans. R. Soc. 170 (1879) 231–256.
[19] P.E. Suetin, B.T. Porodnov, V.G. Chernjak, S.F. Borisov, Poiseuille flow at arbitrary Knudsen numbers and tangential momentum accommodation, J. Fluid Mech. 60 (1973) 581.
[20] B.T. Porodnov, P.E. Suetin, S.F. Borisov, V.D. Akinshin, Experimental investigation of rarefied gas flow in different channels, J. Fluid Mech. 64 (1974) 417–438.
[21] S. Varoutis, S. Naris, V. Hauer, C. Day, D. Valougeorgis, Computational and experimental study of gas flows through long channels of various cross sections in the whole range of the Knudsen number, J. Vac. Sci. Technol. A: Vac. Surf. Films 27 (2009) 89–100.
[22] I.A. Graur, P. Perrier, W. Ghozlani, J.G. Méolans, Measurements of tangential momentum accommodation coefficient for various gases in plane microchannel, Phys. Fluids 21 (2009) 102004.
[23] O.V. Sazhin, S.F. Borisov, F. Sharipov, Accommodation coefficient of tangential momentum on atomically clean and contaminated surfaces, J. Vac. Sci. Technol. A Vac. Surf. Films 19 (2001) 2499–2503.
[24] A. Ebrahimi, V. Shahabi, E. Roohi, Pressure-driven nitrogen flow in divergent microchannels with isothermal walls, Appl. Sci. 11 (2021) 3602.
[25] B. John, X.-J. Gu, D.R. Emerson, Nonequilibrium gaseous heat transfer in pressure-driven plane Poiseuille flow, Phys. Rev. E 88 (2013) 013018.
[26] T. Ohwada, Heat flow and temperature and density distributions in a rarefied gas between parallel plates with different temperatures. Finite-difference analysis of the nonlinear Boltzmann equation for hard-sphere molecules, Phys. Fluids 8 (1996) 2153–2160.
[27] M.T. Ho, I. Graur, Heat transfer through rarefied gas confined between two concentric spheres, Int. J. Heat. Mass Transf. 90 (2015) 58–71.
[28] F.O. Goodman, Dynamics of Gas-Surface Scattering, Elsevier Science, Saint Louis, 2014.
[29] C. Cercignani, M. Lampis, Kinetic models for gas-surface interactions, Transp. Theory Stat. Phys. 1 (1971) 101–114.
[30] F. Sharipov, Application of the Cercignani–Lampis scattering kernel to calculations of rarefied gas flows. I. Plane flow between two parallel plates, Eur. J. Mech. B/Fluids 21 (2002) 113–123.
[31] R.G. Lord, Some extensions to the Cercignani–Lampis gas–surface scattering kernel, Phys. Fluids A Fluid Dyn. 3 (1991) 706–710.
[32] T. Liang, Q. Li, W. Ye, Performance evaluation of maxwell and Cercignani-Lampis gas-wall interaction models in the modeling of thermally driven rarefied gas transport, Phys. Rev. E 88 (2013) 013009.
[33] S. Pantazis, S. Varoutis, V. Hauer, C. Day, D. Valougeorgis, Gas-surface scattering effect on vacuum gas flows through rectangular channels, Vacuum 85 (2011) 1161–1164.
[34] T. Edmonds, J.P. Hobson, A study of thermal transpiration using ultrahigh-vacuum techniques, J. Vac. Sci. Technol. 2 (1965) 182–197.
[35] O. Sazhin, A. Kulev, S. Borisov, S. Gimelshein, Numerical analysis of gas–surface scattering effect on thermal transpiration in the free molecular regime, Vacuum 82 (2007) 20–29.
[36] F. Sharipov, Application of the Cercignani–Lampis scattering kernel to calculations of rarefied gas flows. III. Poiseuille flow and thermal creep through a long tube, Eur. J. Mech. - B/Fluids 22 (2003) 145–154.
[37] R.D.M. Garcia, C.E. Siewert, The linearized Boltzmann equation with Cercignani–Lampis boundary conditions: basic flow problems in a plane channel, Eur. J. Mech. - B/Fluids 28 (2009) 387–396.
[38] L. Wu, H. Struchtrup, Assessment and development of the gas kinetic boundary condition for the Boltzmann equation, J. Fluid Mech. 823 (2017) 511–537.
[39] T. Basdanis, G. Tatsios, D. Valougeorgis, Gas-surface interaction in rarefied gas flows through long capillaries via the linearized Boltzmann equation with various boundary conditions, Vacuum 202 (2022) 111152.
[40] M. Vargas, S. Stefanov, D. Valougeorgis, On the effect of the boundary conditions and the collision model on rarefied gas flows, Pac. Grove Calif. (2011) 354–359.
[41] S. Pantazis, D. Valougeorgis, Heat transfer through rarefied gases between coaxial cylindrical surfaces with arbitrary temperature difference, Eur. J. Mech. B/Fluids 29 (2010) 494–509.
[42] F. Sharipov, Application of the Cercignani–Lampis scattering kernel to calculations of rarefied gas flows. II. Slip and jump coefficients, Eur. J. Mech. B/Fluids 22 (2003) 133–143.
[43] T. Basdanis, D. Valougeorgis, F. Sharipov, Viscous and thermal velocity slip coefficients via the linearized Boltzmann equation with ab initio potential, Microfluid Nanofluid 27 (2023) 75.
[44] S.K. Peravali, V. Jafari, A.K. Samanta, J. Küpper, P. Neumann, M. Breuer, Accuracy and Performance Evaluation of Low Density Internal and External Flows using CFD and DSMC, (2024).
[45] D. Kalempa, F. Sharipov, Drag and thermophoresis on a sphere in a rarefied gas based on the Cercignani–Lampis model of gas–surface interaction, J. Fluid Mech. 900 (2020) A37.
[46] F. Sharipov, D. Kalempa, Numerical modeling of the sound propagation through a rarefied gas in a semi-infinite space on the basis of linearized kinetic equation, J. Acoust. Soc. Am. 124 (2008) 1993–2001.
[47] D. Kalempa, F. Sharipov, Thermophoretic force on a sphere of arbitrary thermal conductivity in a rarefied gas, Vacuum 201 (2022) 111062.
[48] N.N. Nguyen, I. Graur, P. Perrier, S. Lorenzani, Variational derivation of thermal slip coefficients on the basis of the Boltzmann equation for hard-sphere molecules and Cercignani–Lampis boundary conditions: comparison with experimental results, Phys. Fluids 32 (2020) 102011.
[49] R. Brancher, M.V. Johansson, P. Perrier, I. Graur, Measurements of pressure gradient and temperature gradient driven flows in a rectangular channel, J. Fluid Mech. 923 (2021) A35.
[50] F. Sharipov, M.R. Moldover, Energy accommodation coefficient extracted from acoustic resonator experiments, J. Vac. Sci. Technol. A: Vac. Surf. Films 34 (2016) 061604.
[51] B.T. Porodnov, A.N. Kulev, F.T. Tuchvetov, Thermal transpiration in a circular capillary with a small temperature difference, J. Fluid Mech. 88 (1978) 609–622.
[52] T. Ewart, P. Perrier, I. Graur, J. Gilbert Méolans, Mass flow rate measurements in gas micro flows, Exp. Fluids 41 (2006) 487–498.
[53] T. Ewart, P. Perrier, I. Graur, J.G. Méolans, Tangential momemtum accommodation in microtube, Microfluid Nanofluid 3 (2007) 689–695.
[54] T. Ewart, P. Perrier, I.A. Graur, J.G. Méolans, Mass flow rate measurements in a microchannel, from hydrodynamic to near free molecular regimes, J. Fluid Mech. 584 (2007) 337–356.

[55] M. Rojas Cardenas, I. Graur, P. Perrier, J.G. Meolans, Thermal transpiration flow: a circular cross-section microtube submitted to a temperature gradient, Phys. Fluids 23 (2011) 031702.
[56] M. Rojas-Cárdenas, I. Graur, P. Perrier, J.G. Méolans, Time-dependent experimental analysis of a thermal transpiration rarefied gas flow, Phys. Fluids 25 (2013) 072001.
[57] H. Yamaguchi, M. Rojas-Cárdenas, P. Perrier, I. Graur, T. Niimi, Thermal transpiration flow through a single rectangular channel, J. Fluid Mech. 744 (2014) 169–182.
[58] H. Yamaguchi, P. Perrier, M.T. Ho, J.G. Méolans, T. Niimi, I. Graur, Mass flow rate measurement of thermal creep flow from transitional to slip flow regime, J. Fluid Mech. 795 (2016) 690–707.
[59] T. Verbovšek, B.Š. Batič, J. Šetina, Investigation into the influence of surface conditions on the tube conductance for the molecular flow regime, Vacuum 161 (2019) 150–156.
[60] T. Missoni, H. Yamaguchi, I. Graur, S. Lorenzani, Extraction of tangential momentum and normal energy accommodation coefficients by comparing variational solutions of the boltzmann equation with experiments on thermal creep gas flow in microchannels, Fluids 6 (2021) 445.
[61] M. Epstein, A model of the wall boundary condition in kinetic theory, AIAA J. 5 (1967) 1797–1800.
[62] H. Struchtrup, Maxwell boundary condition and velocity dependent accommodation coefficient, Phys. Fluids 25 (2013) 112001.
[63] E.M. Shakhov, Generalization of the Krook kinetic relaxation equation, Fluid Dyn. 3 (1972) 95–96.
[64] R.W. Walter, L. Huyse, Uncertainty analysis for fluid mechanics with applications., No. ICASE-2002-1 National Aeronautics and Space Administration, Hampton VA Langley Research Center, 2002.
[65] G. Tatsios, D. Valougeorgis, Uncertainty analysis of computed flow rates and pressure differences in rarefied pressure and temperature driven gas flows through long capillaries, Eur. J. Mech. B/Fluids 79 (2020) 190–201.
[66] F. Sharipov, Rarefied Gas Dynamics: Fundamentals for Research and Practice, Wiley-VCH Verlag GmbH & Co. KGaA, Weinheim, 2016.
[67] S. Pantazis, Simulation of transport phenomena in conditions far from thermodynamic equilibrium via kinetic theory with applications in vacuum technology and MEMS, Ph.D. Thesis, University of Thessaly, Department of Mechanical Engineering, 2011.
[68] J.M. Hammersley, D.C. Handscomb, Monte Carlo methods, Reprint, Chapman and Hall, London, 1992.
[69] A. Agrawal, S.V. Prabhu, Deduction of slip coefficient in slip and transition regimes from existing cylindrical Couette flow data, Exp. Therm. Fluid Sci. 32 (2008) 991–996.
[70] D.J. Alofs, G.S. Springer, Cylindrical couette flow experiments in the transition regime, Phys. Fluids 14 (1971) 298–305.
[71] G. Breyiannis, S. Varoutis, D. Valougeorgis, Rarefied gas flow in concentric annular tube: estimation of the Poiseuille number and the exact hydraulic diameter, Eur. J. Mech. B/Fluids 27 (2008) 609–622.
[72] F. Sharipov, Rarefied gas flow through a long tube at any temperature ratio, J. Vac. Sci. Technol. A: Vac. Surf. Films 14 (1996) 2627–2635.
[73] I. Graur, F. Sharipov, Non-isothermal flow of rarefied gas through a long pipe with elliptic cross section, Microfluid Nanofluid 6 (2009) 267–275.